Annual Report

Pseudomorphic Semiconducting Heterostructures from Combinations of AlN, GaN and Selected SiC Polytypes: Theoretical Advancement and its Coordination with Experimental Studies of Nucleation, Growth, Characterization and Device Development

Supported under Grant #N00014-90-J-1427
Department of the Navy
Office of the Chief of Naval Research
Report for the period January 1, 1992–December 31, 1992

Robert F. Davis, K. S. Ailey-Trent, R. S. Kern, D. Kester,
R. Patterson, L. B. Rowland, S. Tanaka, and C. Wang
Materials Science and Engineering Department
North Carolina State University
Campus Box 7907
Raleigh, NC 27695-7907

December 1992

REPORT DOCUMENTATION PAGE

Form Approved
OMB No 0704 0188

1. AGENCY USE ONLY (Leave blank)	2. REPORT DATE	3. REPORT TYPE AND DATES COVERED
	December 1992	Annual 1/1/92–12/31/92

4. TITLE AND SUBTITLE
Pseudomorphic Semiconducting Heterostructures from Combinations of AlN, GaN and Selected SiC Polytypes: Theoretical Advancements and its Coordination with Experimental Studies

5. FUNDING NUMBERS
414s007---01
1114ss
N00179
N66005
4B855

6. AUTHOR(S)
Robert F. Davis

7. PERFORMING ORGANIZATION NAME(S) AND ADDRESS(ES)
North Carolina State University
Hillsborough Street
Raleigh, NC 27695

8. PERFORMING ORGANIZATION REPORT NUMBER
N00014-90-J-1427

9. SPONSORING/MONITORING AGENCY NAME(S) AND ADDRESS(ES)
Department of the Navy
Office of the Chief of Naval Research
800 North Quincy, Code 1513:CMB
Arlington, VA 22217-5000

10. SPONSORING/MONITORING AGENCY REPORT NUMBER

11. SUPPLEMENTARY NOTES

12a. DISTRIBUTION/AVAILABILITY STATEMENT
Approved for Public Release—Distribution Unlimited

12b. DISTRIBUTION CODE

13. ABSTRACT *(Maximum 200 words)*

Pseudomorphic bilayer structures containing β(3C)-SiC and 2H-AlN have been grown for the first time on vicinal α(6H)-SiC(0001) homoepitaxial layers at 1050°C by plasma-assisted, gas source molecular beam epitaxy. High energy electron diffraction and cross-sectional high-resolution transmission electron microscopy showed all layers to be monocrystalline. The AlN layers were uniform in thickness. Defects in these layers were initiated at steps on the 6H-SiC film. Pseudomorphic layers of GaN have also been deposited on thin films of AlN grown on α(6H)-SiC(0001) and sapphire(0001). This was achieved by preventing the formation of a thin amorphous layer on both substrates via reaction with the active N species from the ECR plasma source. The p-type and n-type doping of GaN during deposition with Mg and Si, respectively, has also been achieved for the first time. The resistivity, Hall mobility and carrier concentration of the p-type material were 0.5 ohm·cm, 10 $cm^2/V \cdot s$ and 1×10^{18} cm^{-3}, respectively. Layers of cubic-BN have been achieved on Si(100) and diamond(100); however, they were occurred as a final step in a sequence; wherein, the prior layers consisted of a-BN and h-BN.

14. SUBJECT TERMS	15. NUMBER OF PAGES
pseudomorphic structures, beta-SiC, GaN, AlN, alpha-SiC, gas-source molecular beam epitaxy, p-type GaN, n-type GaN, resistivity, Hall mobility, carrier concentration, cubic-BN, Si(100), diamond(100)	63
	16. PRICE CODE

17. SECURITY CLASSIFICATION OF REPORT	18. SECURITY CLASSIFICATION OF THIS PAGE	19. SECURITY CLASSIFICATION OF ABSTRACT	20. LIMITATION OF ABSTRACT
UNCLAS	UNCLAS	UNCLAS	SAR

Table of Contents

I. Introduction

The advent of techniques for growing semiconductor multilayer structures with layer thicknesses approaching atomic dimensions has provided new systems for both basic physics studies and device applications. Most of the research involving these structures has been restricted to materials with lattice constants that are equal within $\simeq 0.1\%$. However it is now recognized that interesting and useful pseudomorphic structures can also be grown from a much larger set of materials that have lattice-constant mismatches in the percent range. Moreover, advances in computer hardware and software as well as the development of theoretical structural and molecular models applicable for strained layer nucleation, growth and property prediction have occurred to the extent that the field is poised to expand rapidly. It is within this context that the research described in this report is being conducted. The materials systems of concern include combinations of the direct bandgap materials of AlN and GaN and selected, indirect bandgap SiC polytypes.

The extremes in thermal, mechanical, chemical and electronic properties of SiC allow the types and numbers of current and conceivable applications of this material to be substantial. However, a principal driving force for the current resurgence of interest in this material, as well as AlN and GaN, is their potential as hosts for high power, high temperature microelectronic and optoelectronic devices for use in extreme environments. The availability of thin film heterostructural combinations of these materials will substantially broaden the applications potential for these materials. The pseudomorphic structures produced from these materials will be unique because of their chemistry, their wide bandgaps, the availability of indirect/direct bandgap combinations, their occurrence in cubic and hexagonal forms and the ability to tailor the lattice parameters and therefore the amount of strain and the physical properties via solid solutions composed of the three components.

The research described in the following sections is concerned with the pseudomorphic nature and microstructural character of (1) AlN/SiC, (2) AlN/GaN, (3) BN/Si and BN/diamond layered assemblies. These sections detail the procedures, results, discussions of these results, conclusions and plans for future research. Each subsection is self-contained with its own figures, tables, and references.

II. Aluminum Nitride/Silicon Carbide Multilayer Heterostructure Produced by Plasma-Assisted Gas-Source Molecular Beam Epitaxy

Submitted for Consideration for Publication
to
Applied Physics Letters

L. B. Rowland*
R. S. Kern
S. Tanaka
Robert F. Davis

North Carolina State University
Department of Materials Science and Engineering
Box 7907
Raleigh, North Carolina 27695-7907

November, 1992

ABSTRACT

Pseudomorphic bilayer structures containing β(3C)-SiC and 2H-AlN have been grown on vicinal α(6H)-SiC(0001) homoepitaxial layers at 1050°C by plasma-assisted, gas source molecular beam epitaxy. High energy electron diffraction and cross-sectional high-resolution transmission electron microscopy showed all layers to be monocrystalline. The AlN layers were uniform in thickness. Defects in these layers were initiated at steps on the 6H-SiC film. The 3C-SiC layers contained a high density of stacking faults and microtwins caused primarily by the interfacial stresses generated by the mismatch in lattice parameters between AlN and β-SiC coupled with the very low stacking fault energy of SiC. This is the first report of the deposition of single crystal SiC/AlN/SiC thin film heterostructures on any substrate as well as the first report of the epitaxial growth of single crystal layers of binary materials with three different crystal structures.

*Present Address
Naval Research Laboratory, Code 6861
4555 Overlook Av., SW
Washington, DC 20375-5320

Interest in wide bandgap semiconductors for high-temperature and high-power electronic and short-wavelength optoelectronic applications has increased markedly within the past several years. Two materials which have generated much interest in this regard are SiC and AlN. The former occurs in over 250 polytypes which differ only in their stacking sequence along the closest-packed direction. The most common of these are the cubic 3C and the hexagonal 6H, where the number refers to the number of Si and C bilayers necessary to produce a unit cell in the direction of closest packing. The 3C polytype is also referred to as β-SiC. All other forms are known collectively as α-SiC. The bandgap (3.0 eV for 6H and 2.28 eV for 3C at room temperature) is indirect in all polytypes; thus, they cannot be used alone for laser applications.

Aluminum nitride has considerable potential for electronic and ultraviolet optoelectronic applications, particularly in severe environments, due to its large and direct bandgap (6.28 eV at 300°C), high melting point (in excess of 2000°C), high thermal conductivity (3.2 W/cm·K), and low dielectric constant (ε=9.0). It typically forms in the wurtzite (2H) structure; however, the cubic, zincblende (3C) phase has recently been produced via molecular beam epitaxy (MBE) techniques [1, 2]. Additional characteristics of the 2H polytype include a high resistivity and ease of oxygen incorporation during growth.

Epitaxial wurtzitic AlN has been deposited previously on SiC substrates [3–5]. Chu et al. [3] obtained monocrystalline AlN layers of up to 25 μm thickness on hexagonal SiC{0001} substrates by chemical vapor deposition (CVD) from 1200-1250°C. Sitar et al. [4] used an electron cyclotron resonance (ECR) plasma for decomposition of N_2 and Al and Ga effusion cells for growth of AlN/GaN superlattices by plasma-assisted, gas source MBE on α(6H)-SiC(0001) and Al_2O_3(0001) at 600°C. The thickness range of the AlN layers was 0.5–20nm. However, the properties of the individual AlN layers were not examined. Yoshida et al. [5] also employed gas–source MBE and the sources of solid Al and NH_3 to deposit single crystal AlN films on Si(111) and Al_2O_3(0001) and (01$\bar{1}$2) at 1000-1200°C. They noted their films were much smoother than CVD-grown material and rivaled bulk single crystal AlN. Conversely, Rutz and Cuomo [6] reported the deposition of monocrystalline SiC on a single crystal AlN film by pyrolysis of a SiC target at 1860°C. The AlN substrate was previously formed at 1000°C by reactive rf sputtering on a W(111) single crystal. However, thin-film growth of AlN/SiC/AlN or SiC/AlN/SiC heterostructures has not been reported to date.

Stable pseudomorphic heterostructures of AlN and SiC are feasible because of their similarity in crystal structure, lattice parameter and thermal expansion behavior. Theory regarding the electronic structure and bonding at SiC/AlN interfaces has been developed [7]. Critical layer thicknesses prior to misfit dislocation formation at pseudomorphic interfaces of cubic AlN and cubic SiC have been calculated [8]. Superlattices of these materials would have a different band structure than either constituent element because the Brillouin zone is reduced

in size in the direction normal to the interfaces, and certain superlattice states occur at different points in k space than the corresponding bulk material [9]. This may allow the resultant superlattice to have a direct band transition.

In the present research multiple layers of AlN and SiC were grown using a specially designed plasma-assisted gas-source molecular beam epitaxy (PAGSMBE) system. A schematic of this equipment is shown in Figure 1. This system is similar to that described previously for SiC MBE growth [10]. The precursors used for Si and C were Si_2H_6 and C_2H_4 (both 99.99% pure), respectively. Solid Al (99.999% pure) was evaporated from a standard effusion cell. Nitrogen was obtained by electron cyclotron resonance (ECR) plasma decomposition of N_2 (99.9995% pure). The system base and working pressures were 10^{-9} and 3×10^{-5} torr, respectively. Vicinal 6H-SiC(0001) wafers oriented 3-4° towards [11$\bar{2}$0] and containing a thermally oxidized(50nm) 0.8 μm epitaxial 6H-SiC layer deposited via CVD were obtained from Cree Research, Inc. and used as substrates in this research These substrates were chemically cleaned prior to growth in a 10% HF solution for five min. to remove the oxide, rinsed in DI H_2O for two min, immediately loaded into the growth system and heated for five min at the growth temperature of 1050°C. Additional growth conditions are listed in Table I.

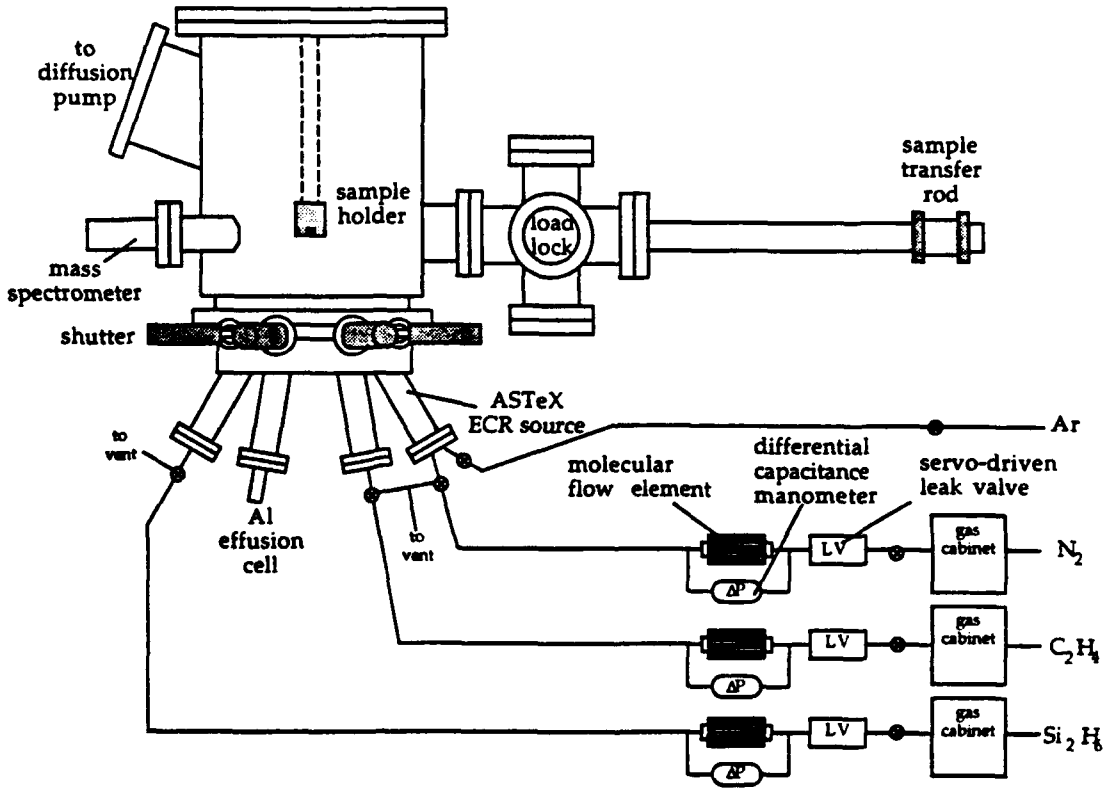

Figure 1. Schematic of gas-source molecular beam epitaxy system use to deposit the SiC and AlN films in this research.

Table I. Growth Conditions for the AlN and SiC Layers

AlN	
Growth temperature	1050°C
Nitrogen pressure	1.5×10^{-4} torr
Nitrogen flow rate	8 sccm
Microwave power	100 W
Growth rate	26 nm/hr
SiC	
Growth temperature	1050°C
Disilane flow rate	0.10 sccm
Ethylene flow rate	0.20 sccm
Growth rate	6.2 nm/hr

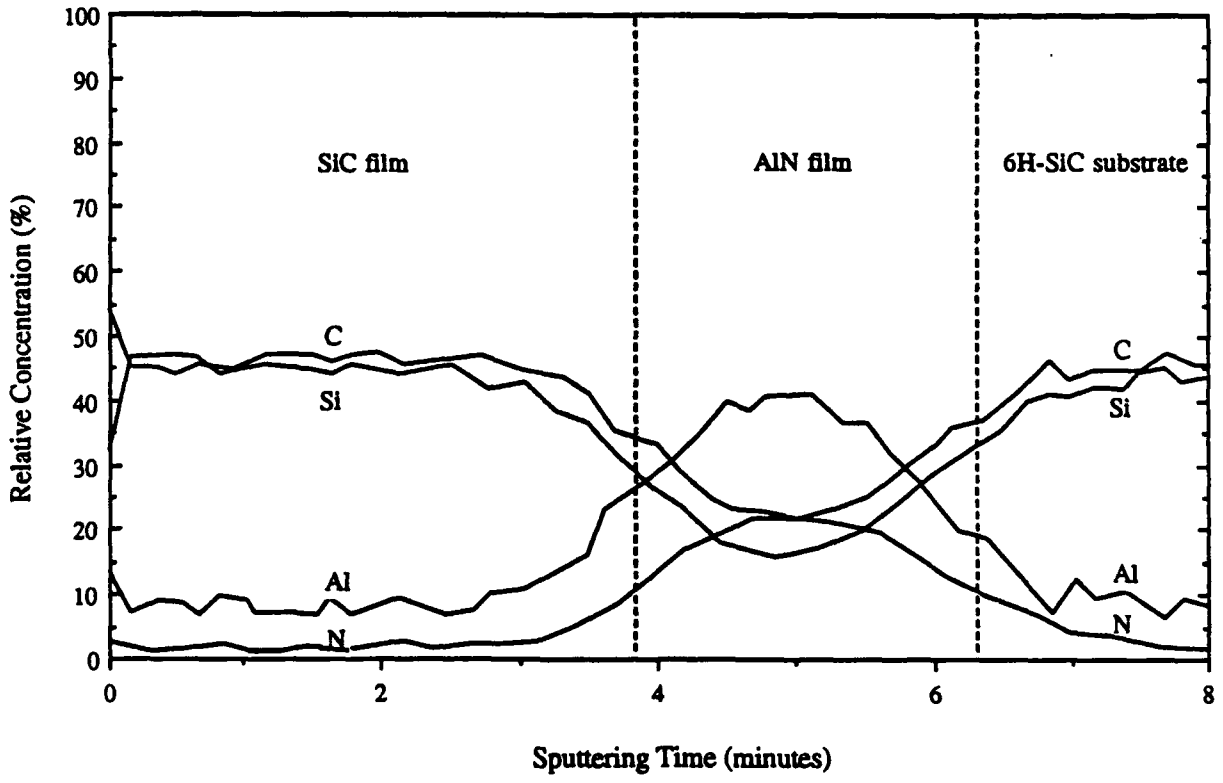

Figure 2. Auger depth profile of representative SiC/AlN/SiC multilayer heterostructure.

Reflection high-energy electron diffraction (RHEED) was used as an indicator of the quality and crystal structure of the resultant films. Figure 3 shows representative RHEED patterns for (a) the final growth surfaces of the films of AlN ([10$\bar{1}$0] azimuth) and (b) SiC ([110] aximuth). These patterns also show that both films were monocrystalline with the AlN having the 2H structure and the SiC the 3C modification, as indicated by the azimuthal assignments. The RHEED pattern of the top SiC layer also contains additional spots, as denoted by arrows in Figure 3(b). This pattern is fully indexed in Figure 4. It is probable that these extra spots arise from double positioning boundaries (DPBs). These incoherent twin boundaries occur when 3C-SiC (111) is grown on Si (111) [11] or on-axis 6H-SiC [12] because two different orientations, rotated 60° from each other, are present which have close-packed directions aligned in the interface. These different orientations differ in the cubic stacking sequence, as one orientation has an ...ABCABC... stacking sequence and the other has an ...ACBACB...stacking sequence. Extra reflections in the [110] RHEED pattern due to double positioning twins would either coincide with those of the film or be displaced by 1/3[111]. The extra spots present in the figure occur at 1/3 of the distance between adjacent spots in the [111] and [111] directions.

An equivalent interpretation of the RHEED pattern shown in Figure 3(b) is of two interpenetrating [110] RHEED patterns with a misorientation of 180°. This misorientation is caused by reflections from regions with both ...ABCABC... and ...ACBACB... sequences. The effect of each individual stacking sequence as well as the resultant RHEED pattern due to contributions of the two equivalent stacking sequences are shown in Figure 5.

Figure 6 shows a representative HRTEM image of the off-axis 6H-SiC (0001) substrate, the 2H-AlN layer, and the 3C-SiC layer. The interface between the SiC substrate and the AlN is abrupt with little change in contrast across it. The surface of the AlN film is smooth and uniform. The 2H-AlN and 6H-SiC films are in the same orientation in all directions, and the alignment of the atom columns is continuous across the interface. Thus, the AlN film is both epitaxial and pseudomorphic with respect to the substrate. Strain contrast, as evidenced by distortion in the lattice fringes, can be seen near steps in the SiC substrate surface, as denoted by arrows in Figure 6. Dislocations running parallel to the surface which arise from this strain can also be observed at or near each step.

The interface between the AlN and the top 3C-SiC layer is also abrupt, though some regions exist for which the transition between AlN and SiC becomes indiscernible. The lattice structural images show that the SiC layer is indeed cubic as well as epitaxial and pseudomorphic with the AlN. Several <111> stacking faults can be seen in the cubic SiC layer.

Previous PAGSMBE growth in this research of SiC on similar substrates at 1000–1050°C also resulted in 3C-SiC(111). This result, combined with those noted above, suggest that the cubic polytype forms preferentially at these temperatures under the conditions of low growth

(a)

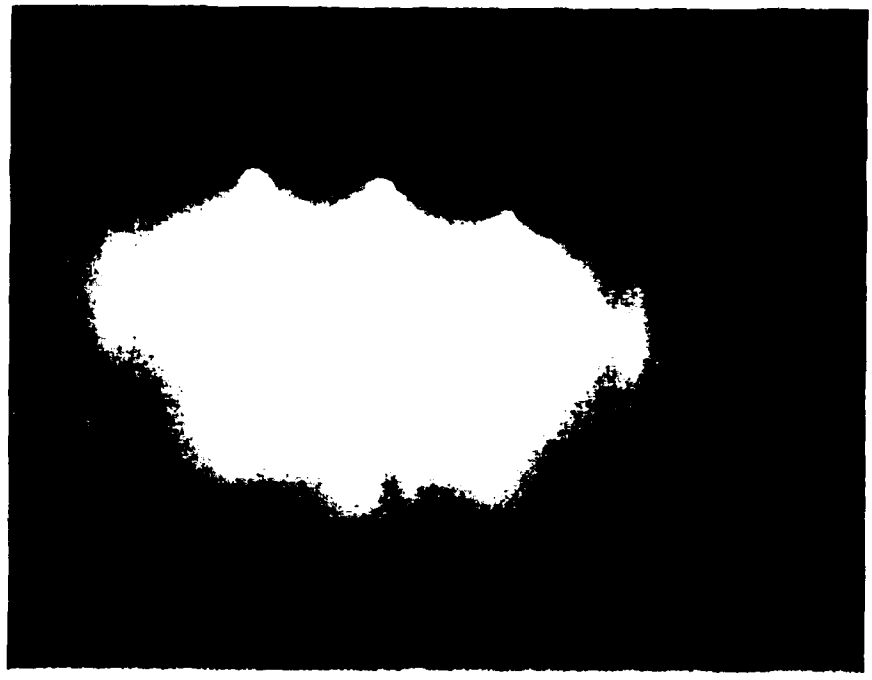

(b)

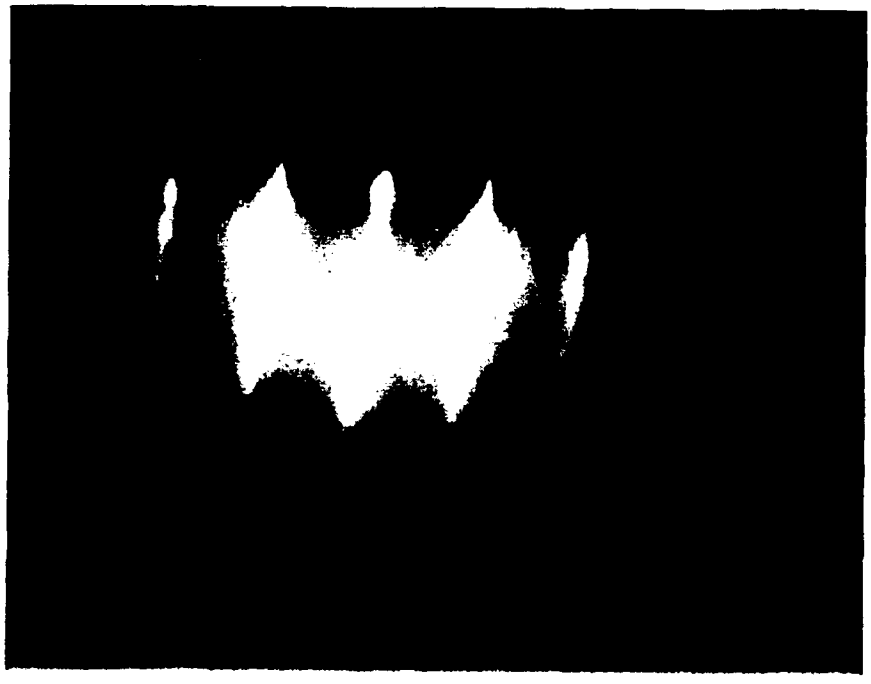

Figure 3. (a) RHEED pattern ([10$\bar{1}$0] azimuth) of the final surface of a monocrystalline 2H-AlN layer grown on α(6H)-SiC epitaxial layer.

(b) RHEED pattern ([110] azimuth) of the final surface of a monocrystalline 3C-SiC layer grown on 2H-AlN film. Arrows denote additional spots in the 3C-SiC layer (see Figures 4 and 5 for indexing).

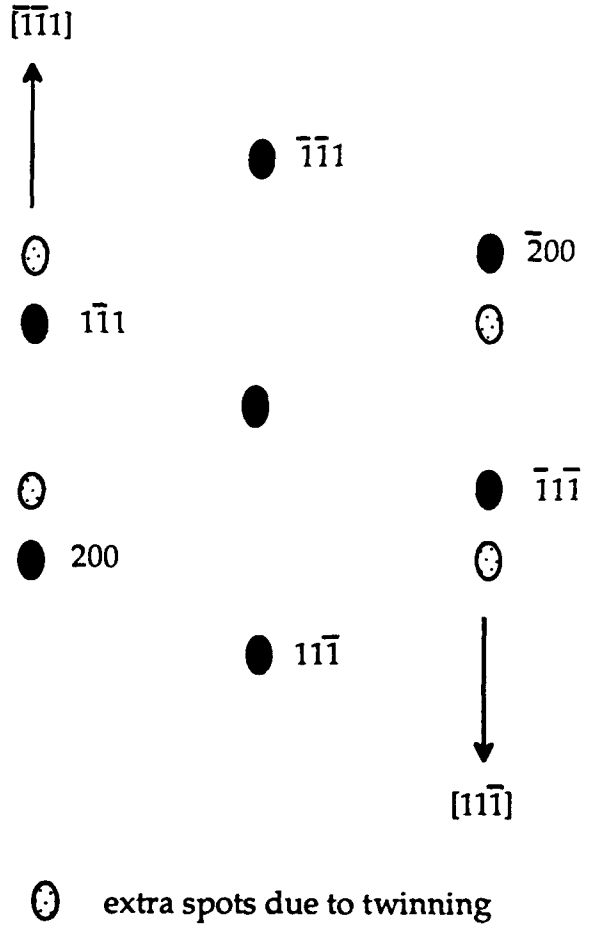

Figure 4. Indexed RHEED pattern ([110] azimuth) of 3C-SiC layer. Lighter spots are twin spots caused by double positioning boundaries.

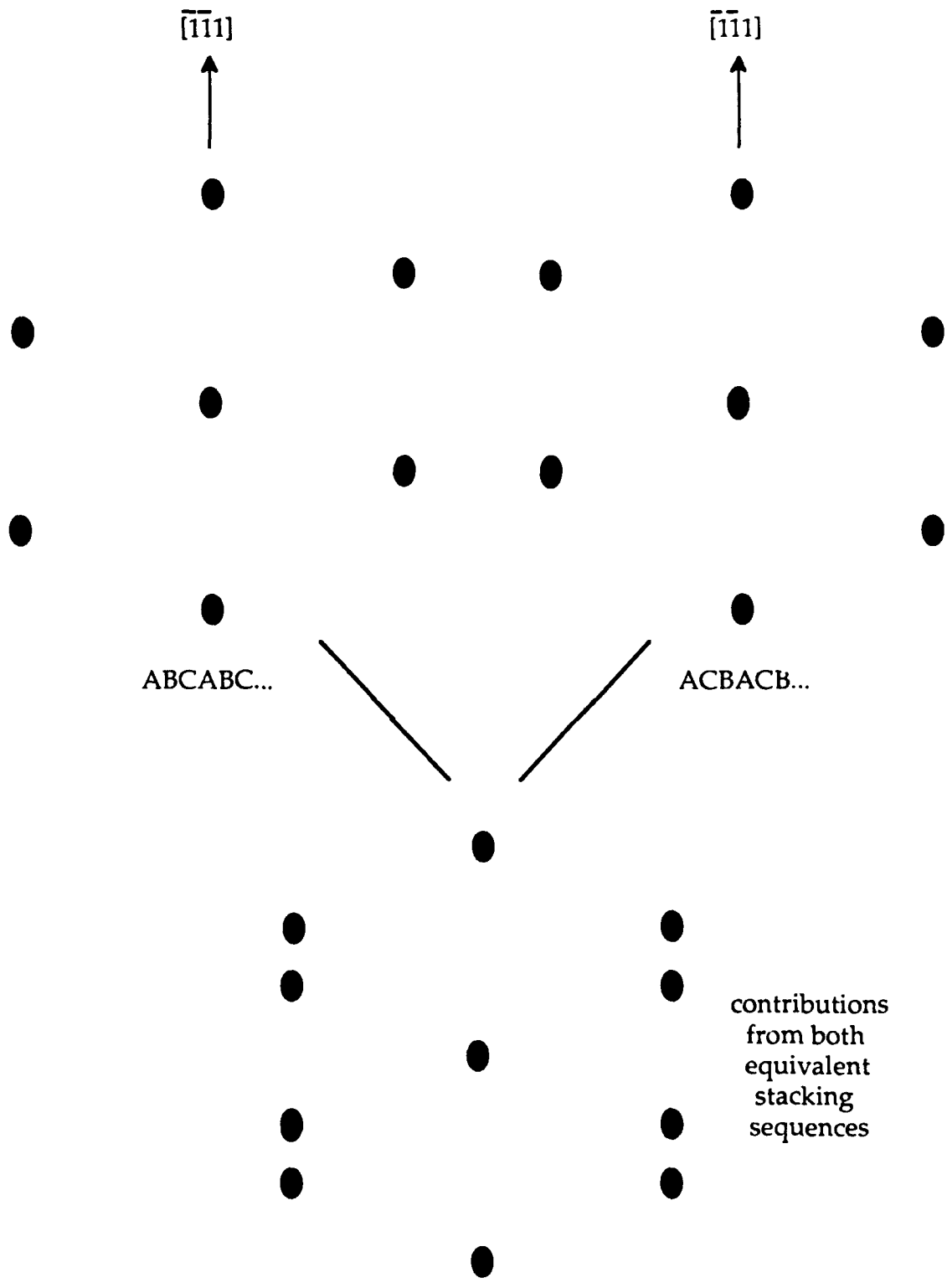

Figure 5. Effect of two equivalent stacking sequences of 3C-SiC (111) on [110] azimuth RHEED pattern.

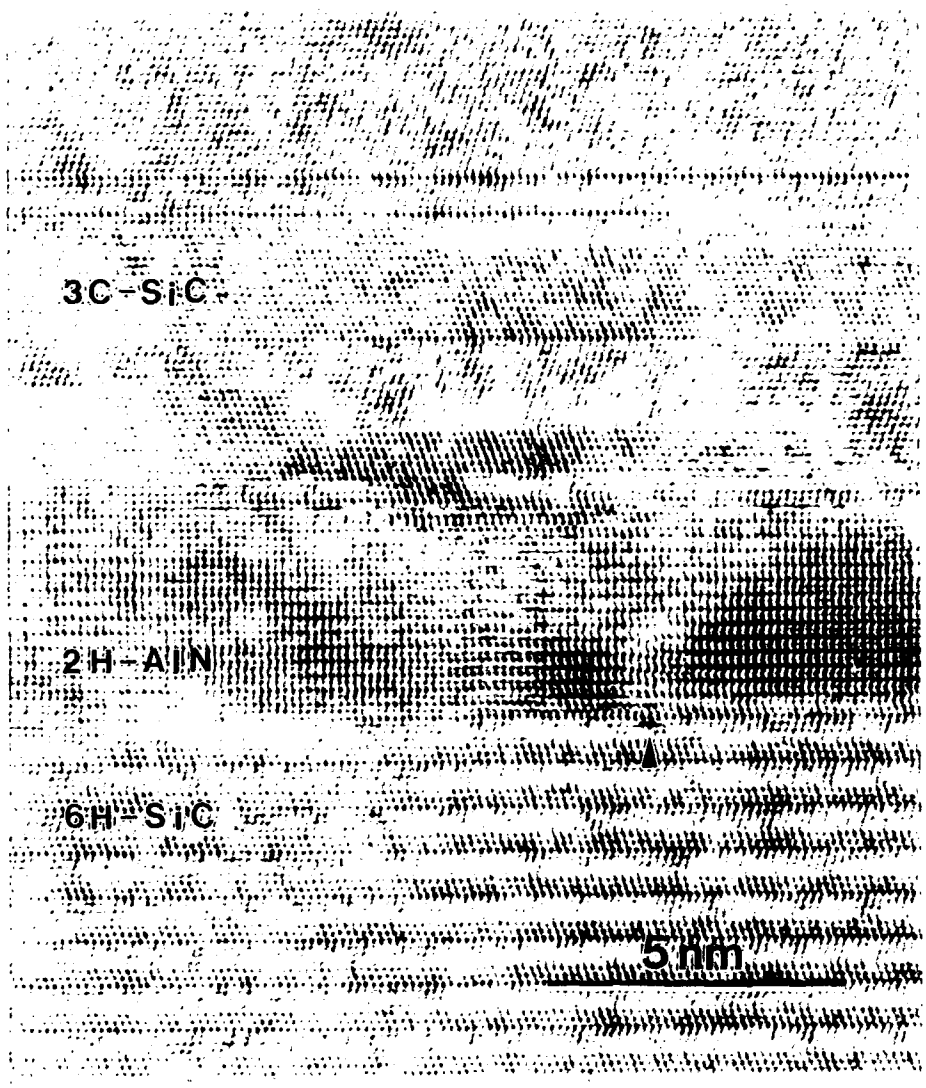

Figure 6. High-resolution transmission electron micrograph of epitaxial, pseudomorphic SiC/AlN/SiC multilayer heterostructure. Arrow shows a position of lattice distortion in the AlN associated with steps contained in and dislocations running parallel to the SiC surface.

rate and high supersaturation used in MBE. However, growth of SiC/AlN heterostructures at higher temperatures may result in hexagonal SiC layers, as atomic mobility on the AlN surface increases and the steps rather than the terraces become the templates for layer-by-layer growth. This trend towards the deposition of hexagonal SiC films at higher temperatures has been reported by several investigators[12-14]. It is also under study in the authors' laboratory and will be reported in the near future.

In summary, thin-film heterostructures composed of 3C-SiC, 2H-AlN and 6H-SiC have been achieved. The 3C-SiC and the AlN layers were grown at 1050°C using PAGSMBE. The diagnostic tools of RHEED and cross-sectional HRTEM showed both of these layers to exist in an epitaxial and pseudomorphic relationship with each other and with the 6H–SiC homoepitaxial layer deposited by CVD. To the authors' knowledge, this is the first report and direct observation of a single crystal SiC/AlN/SiC heterostructure on any substrate. It is also the first known report of the single-crystal growth of layers of binary materials in three different crystal structures (the 6H-SiC epilayer on the SiC wafer is counted in this case). These unique structures, composed of direct (AlN) and indirect (SiC) wide bandgap semiconductor materials undoubtedly possess important electronic, mechanical and thermal properties which are under investigation by the authors at this time.

The authors express their appreciation to the Office of Naval Research for support of this research under Grant #N00014-90-J-1427, to Cree Research, Inc. for the vicinal 6H-SiC wafers and epilayers and to Applied Science and Technology, Inc. for supplying the ECR plasma source. Appreciation is also expressed to S. Rogers for the Auger microprobe analysis.

REFERENCES

1. Z. Sitar, Ph. D. dissertation, North Carolina State University, 1990.
2. S. Strite and H. Morkoç, private communication.
3. T. L. Chu, D. W. Ing, and A. J. Norieka, Solid-State Electron. **10**, 1023 (1967).
4. Z. Sitar, M. J. Paisley, B. Yan, R. F. Davis, J. Ruan, and J. W. Choyke, Thin Solid Films **200**, 311 (1991).
5. S. Yoshida, S. Mizawa, Y. Fujii, S. Takada, H. Hayakawa, S. Gonda, and A. Itoh, J. Vac. Sci. Technol. **16**, 990 (1979).
6. R. F. Rutz and J. J. Cuomo, in *Silicon Carbide-1973*, (U. of South Carolina Press, Columbia, 1974), p. 72.
7. W. R. L. Lambrecht and B. Segall, Phys. Rev. B **43**, 7070 (1991).
8. M. E. Sherwin and T. J. Drummond, J. Appl. Phys. **69**, 8423 (1991).
9. G. C. Osbourn, J. Vac. Sci. Technol. B **1**, 379 (1983).
10. L. B. Rowland, R. S. Kern, S. Tanaka, and R. F. Davis, in *Proceedings of the Fourth International Conference on Amorphous and Crystalline Silicon Carbide* (Springer-Verlag, Berlin), in press.
11. I. H. Khan and R. N. Summergrad, Appl. Phys. Lett. **11**, 12 (1967).
12. H. S. Kong, B. L. Jiang, J. T. Glass, G. A. Rozgonyi, and K. L. More, J. Appl. Phys. **63**, 2645 (1988).
13. R. B. Campbell and T. L. Chu, J. Electrochem. Soc. **113**, 825 (1966).
14. V. J. Jennings, A. Sommer, and H. C. Chang, J. Electrochem. Soc. **113**, 728 (1966).

III. Epitaxial Growth of AlN by Plasma-Assisted Gas-Source Molecular Beam Epitaxy

A Communication
Submitted for Consideration for Publication
to
The Journal of Materials Research

L. B. Rowland*, S. Tanaka, R. S. Kern and Robert F. Davis
Department of Materials Science and Engineering
North Carolina State University
Box 7907
Raleigh, North Carolina 27695-7907

November, 1992

ABSTRACT

Monocrystalline AlN(0001) films with few defects were deposited on vicinal α(6H)-SiC(0001) wafers via plasma-assisted gas-source molecular beam epitaxy within the temperature range of 1050–1200°C. The Al was thermally evaporated from an effusion cell. An electron cyclotron resonance plasma source was used to produce activated nitrogen species. Growth on vicinal Si(100) at 900–1050°C resulted in smooth, highly oriented AlN(0001) films.

*Present Address
Naval Research Laboratory, Code 6861
4555 Overlook Av., SW
Washington, DC 20375-5320

Aluminum nitride possesses a direct bandgap of 6.28 eV at 300 K [1], a melting point in excess of 2275 K [2] and a thermal conductivity of 3.2 W/cm·K [3]. As such, it is a candidate material for high-power and high-temperature microelectronic and optoelectronic applications with the latter employment being particularly important in the ultraviolet region of the spectrum [1]. This material also has the highest reported surface acoustic wave velocity (Raleigh V_R=6–6.2 km/s, V_L=11-12 km/s [4]-[6]) for any material and a substantial electromechanical coupling coefficient (to 1% [7]). These properties strongly indicate that superior surface acoustic wave devices, operational in aggressive media and under extreme conditions both as sensors for high temperatures and pressures and as acousto-optic devices can be developed [8-10]. However, progress regarding these (and other) applications is hampered by the lack of good single crystal material. The primary objective of the research reported below has been to address this issue via the fabrication of thin films of this material via molecular beam epitaxy (MBE) techniques.

In previous studies, mono- and polycrystalline films of AlN have been grown by chemical vapor deposition (CVD) using NH_3 and $Al(CH_3)_3$ or $AlCl_3$ on α(6H)-SiC [11], sapphire [1,9,12], and Si [13-15]. Chu et al. [11] obtained smooth monocrystalline AlN layers to a thickness of 25 μm on α(6H)-SiC{0001} substrates by chemical vapor deposition (CVD) from 1200-1250°C. A high density of defects in these AlN films was revealed by chemical etching. In general, films grown on sapphire and Si substrates possessed a much rougher morphology than those grown on α(6H)-SiC. This occurred very likely because the difference in lattice parameters between AlN and SiC is substantially less than between AlN and sapphire or AlN and Si.

Gas source MBE using electron beam evaporated Al and NH_3 [16] or thermally evaporated Al and plasma-derived activated nitrogen species [17] has also been used for single crystal AlN growth. Yoshida et al. [16] obtained single crystal AlN using an Al effusion cell and NH_3 at 1000-1200°C on Si(111) and Al_2O_3(0001) and (01$\bar{1}$2) and obtained growth rates of up to 1 μm/hr. They contended that their films were much smoother than CVD-grown material and rivaled bulk single crystal AlN. Sitar et al. [17] used an electron cyclotron resonance (ECR) plasma for decomposition of N_2 and Al and Ga effusion cells for growth of AlN/GaN superlattices by plasma-assisted, gas source (PAGSMBE) on α(6H)-SiC (0001) and Al_2O_3 (0001) at 600°C. The thickness range of the AlN layers was 0.5–20nm, as determined by cross-sectional transmission electron microscopy (TEM). However, the properties of the individual AlN layers were not examined.

The approach taken in the present research has also been to use PAGSMBE to achieve surface reactions involving only Al and N in order to minimize the potential for unintentional impurity contamination from the p- and n-type dopants of C and O, respectively. The AlN films were grown on vicinal Si(100) wafers oriented 3.5 ± 0.5° towards [011] at 900-1050°C

and vicinal α(6H)-SiC (0001) oriented 3-4° towards [11$\bar{2}$0] at 1050-1200°C in a PAGSMBE system described previously [18]. These temperatures are higher than necessary for the formation of single crystal AlN. However, they were employed to match the growth temperatures previously determined to be necessary to achieve single crystal films of SiC on Si(100) [18-20] and α(6H)-SiC(0001) substrates [21,22].

Silicon(100) substrates were chemically cleaned using the following steps: (1) H_2SO_4 at 70°C for 5 min, (2) deionized water for 1 min, (3) 1:1 solution (by volume) of NH_4OH and 50% H_2O_2 at 70°C for 5 min, (4) deionized water for 1 min, (5) dip in 10% HF at room temperature, and (6) 2 min rinse in deionized water. Silicon carbide substrates were only subjected to cleaning steps (5) and (6) prior to introduction to the growth system. Thermal desorption of all substrates was also conducted at the growth temperature for 5 min prior to deposition to remove any remaining hydrocarbon and/or oxide contamination. An effusion cell was used for the evaporation of Al (99.999% pure). Reactive nitrogen species were produced via decomposition of N_2 (99.999% pure) in a compact electron cyclotron resonance (ECR) plasma source (Applied Science and Technology, Inc.). The pressure of the introduced N_2 was 1.2-1.5 x 10^{-4} torr. The microwave power supplied to the ECR was 100 W for all depositions.

The crystallography and surface character on the films were initially studied *in situ* using reflection high-energy electron diffraction (RHEED). The microstructure of the final growth surface was investigated using field-emission scanning electron microscopy (SEM). The orientation of the films grown on Si was determined via x-ray diffraction. A more in-depth examination of the crystallinity and the nature and distribution of the line and planar defects in the films deposited on 6H-SiC was conducted using high-resolution transmission electron microscopy (HRTEM). The composition of the films, including any significant impurities, was determined using an Auger electron microprobe.

Figure 1 shows the RHEED patterns ([11$\bar{2}$0] azimuth) of AlN films grown on the 6H-SiC (0001) substrates at (a) 1200°C, (b) 1100°C and (c) 1050°C. These patterns indicate that all the films possess the wurtzite structure and are monocrystalline.

The growth rate versus temperature was essentially constant for a given Al flux. Conversely, changes in the AlN growth rate corresponded directly to changes in the Al flux. A constant Al source temperature and, consequently, a constant Al flux were used at the the three temperatures of growth. An excess of activated nitrogen was present under all conditions. A constant growth rate of ≈0.40 nm/min was obtained at these temperatures.

Scanning Auger analysis of these films detected only Al and N except in a 2 nm surface region where the native oxide (and very likely the hydroxide) had formed during exposure to air. The stoichiometry of these films was very close to that obtained from analysis of high-purity, hot-pressed polycrystalline AlN. Figure 2 shows a HRTEM image of a thin AlN layer

(a)

(b)

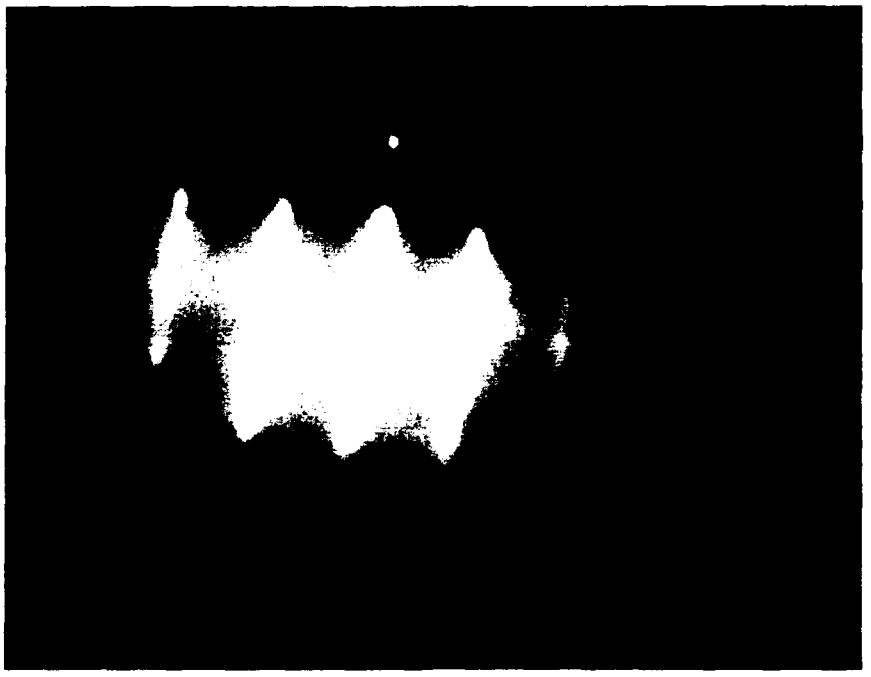

Figure 1. RHEED patterns ([11$\bar{2}$0] azimuth) of AlN grown on vicinal 6H-SiC(0001) at (a) 1200°C, (b) 1100°C, and (c) 1050°C.

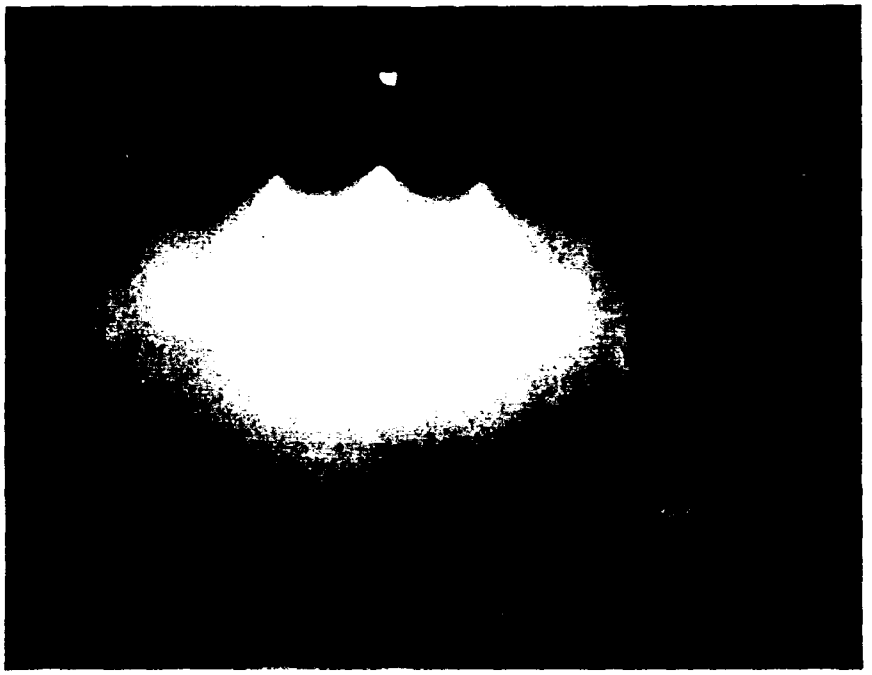

Fig. 1. (c) 1050°C.

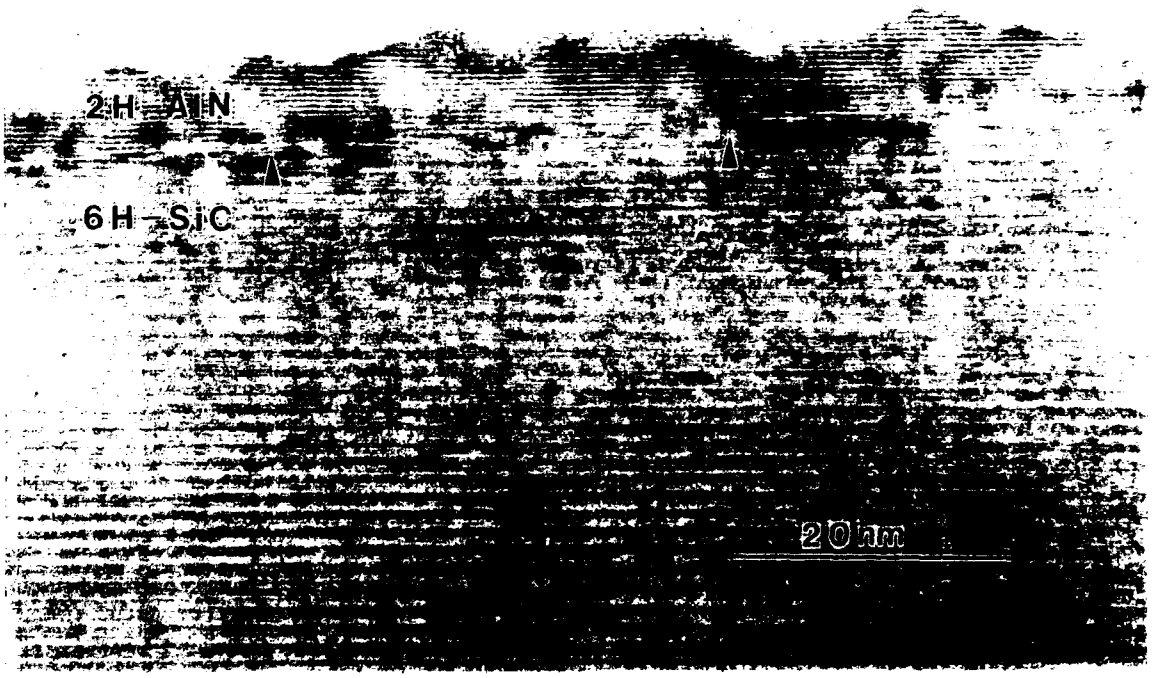

Figure 2. HRTEM micrograph of AlN film grown at 1200°C on vicinal 6H-SiC (0001). Arrows point to areas of lattice distortion in the lattice fringes of the AlN.

deposited on the 6H-SiC at 1200°C. The top surface of the AlN is rough. Few defects are visible away from the interface. At the 2H-AlN/6H-SiC interface, however, strain contrast as evidenced by distortion in the lattice fringes can be seen (denoted by arrows in Figure 2).

A further reduction in temperature to 1050°C also resulted in the deposition of single crystal AlN films (as indicated in Figure 1(c)) having an abrupt interface with the SiC substrates, but with a much smoother final surface, as shown in the SEM micrograph of Figure 3. This essentially featureless microstructure supports the RHEED results. The surface morphology was difficult to observe at much higher magnifications in the SEM due to the insulating nature of both AlN and the SiC substrate. Figure 4 shows a HRTEM image of a film grown at 1050°C capped by a monocrystalline, cubic (zincblende structure) β-SiC(111) film grown in the same experiment. The smooth AlN surface and the abrupt junction with the β-SiC are apparent. Dislocations in the AlN films occurred at surface steps in the 6H-SiC substrate and may be observed in Figure 4 (see arrow). No other defects were observed in this material. The use of nominally on-axis 6H-SiC substrates with widely spaced steps will be studied in the near future to reduce the defects present in these films.

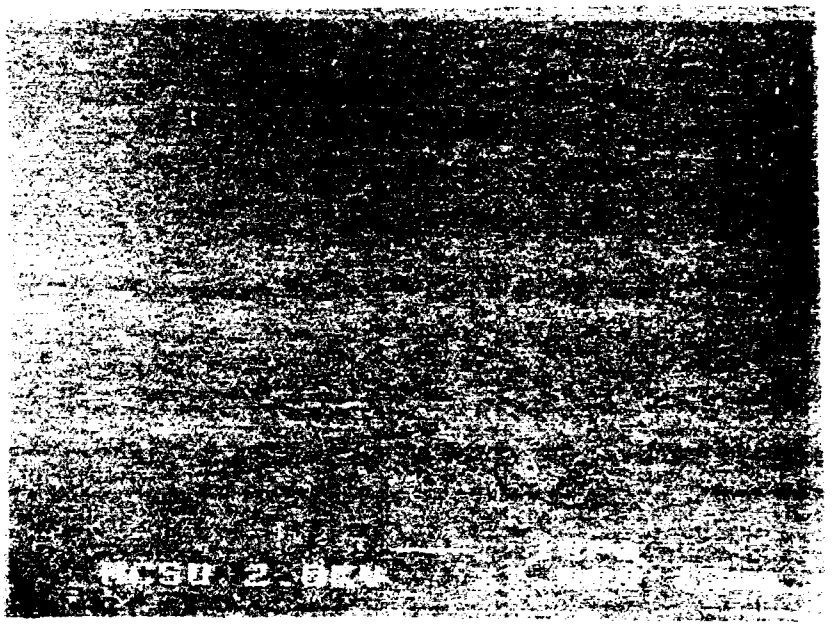

Figure 3. SEM micrograph of the surface morphology of an AlN film grown on vicinal 6H-SiC(0001) at 1050°C.

Figure 5 shows RHEED patterns of AlN layers deposited at 900 and 1050°C on Si(100) substrates. These films have the wurtzite structure and are very well-oriented. There is only a small amount of angular spread in the spots which implies that the films have a small non-epitaxial component. An X-ray diffraction scan of the film grown at 1050°C is shown in

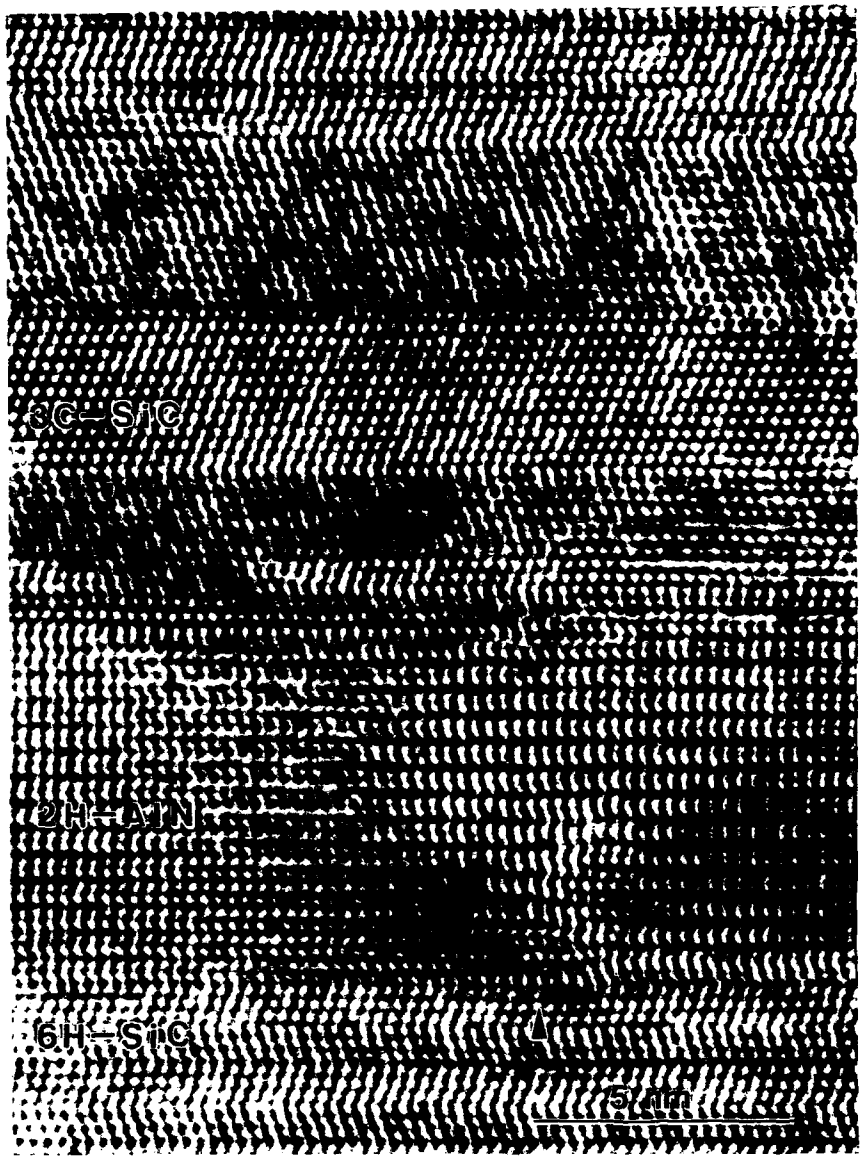

Figure 4. HRTEM micrograph of AlN film grown at 1050°C on vicinal 6H-SiC (0001). Layer above AlN layer is 3C-SiC also grown at 1050°C using gas-source MBE. Arrow points to dislocation in the AlN film at a step on the 6H–SiC surface.

Figure 6. The single (0002) AlN peak supports the RHEED results regarding orientation. The AlN therefore grows with the closest packed plane parallel to the non-closest packed (100) plane in the Si substrate. Figure 7 shows a SEM micrograph of the grown surface at 1050°C. The film is smooth except for occasional small elongated depressions in the surface. The reason for these features has not been determined; however, they may be due to pitting of the Si surface before AlN growth. These films were extremely smooth when compared to those grown by CVD [13-15].

(a)

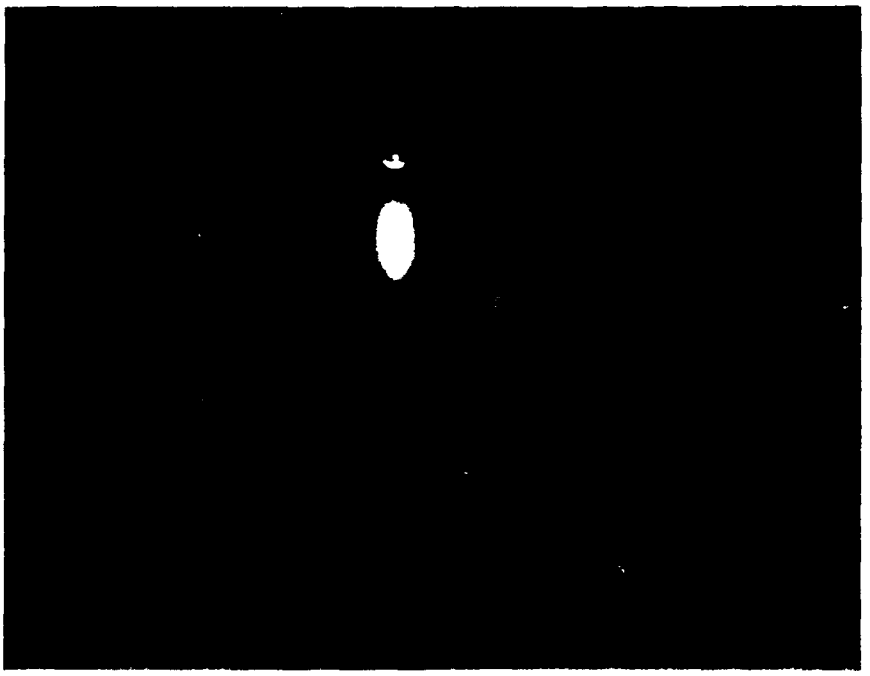

(b)

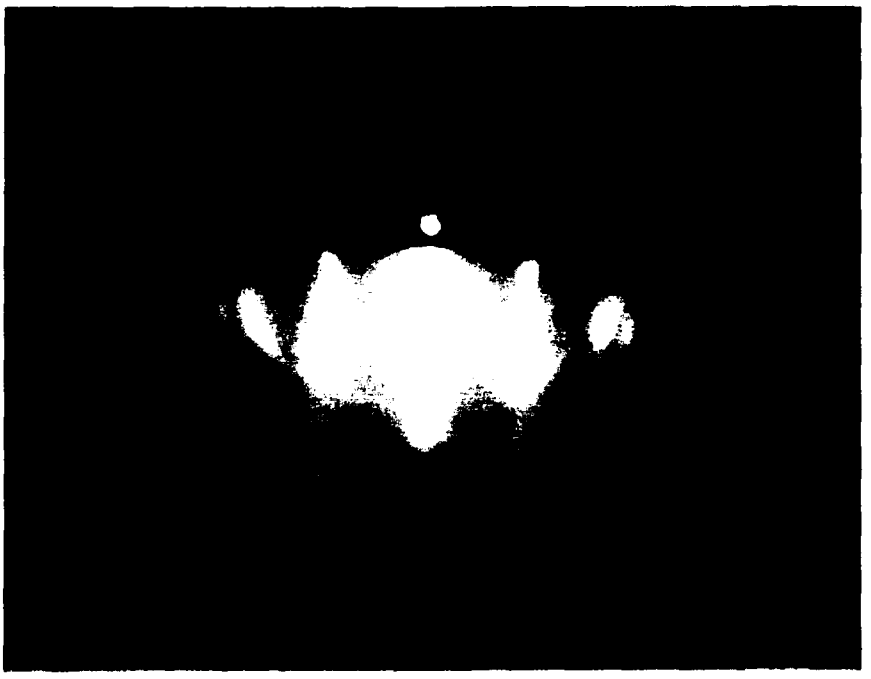

Figure 5. RHEED patterns ([11$\bar{2}$0] azimuth) of AlN films grown on vicinal Si(100) at (a) 900°C and (b) 1050°C.

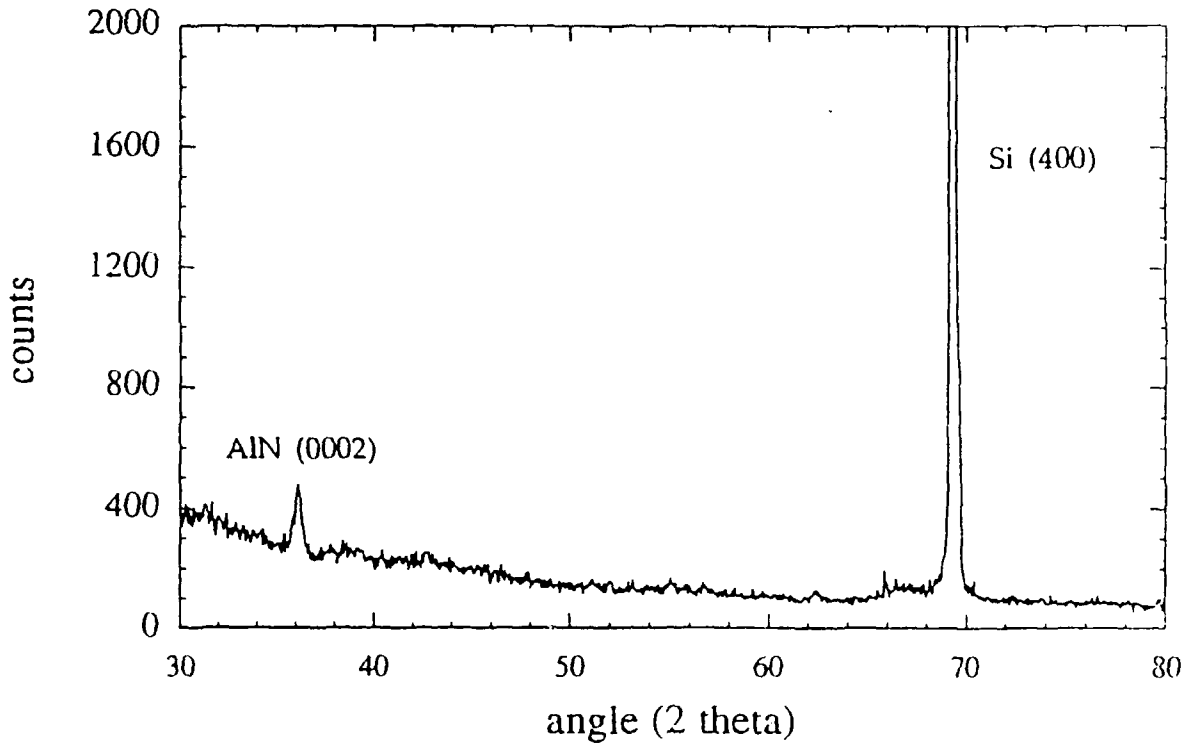

Figure 6. X-ray diffraction spectrum (CuKα) of AlN film on vicinal Si(100) at 1050°C.

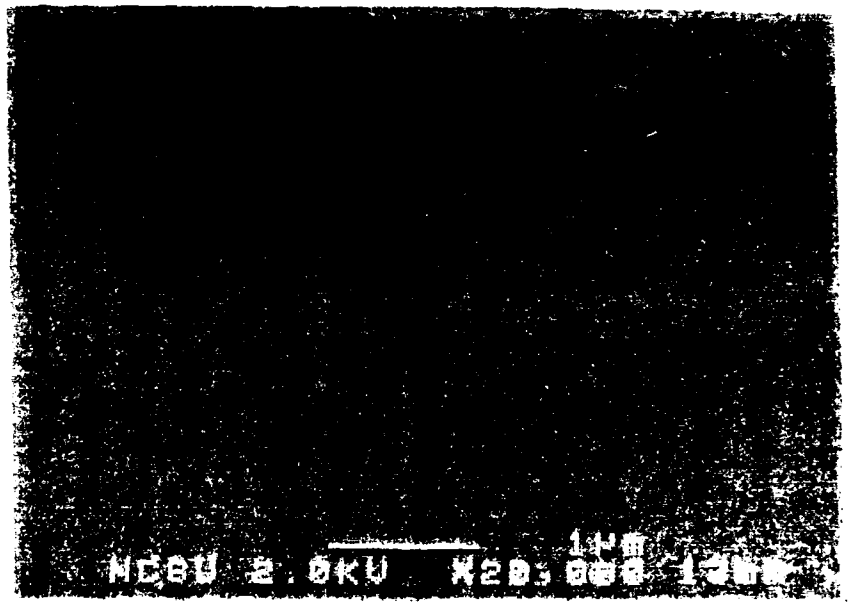

Figure 7. Scanning electron micrograph of surface morphology of AlN grown on vicinal Si(100) at 1050°C.

An orientation of AlN such as $(10\bar{1}0)$ is more likely than (0001) on Si(100), based on crystallographic considerations. The latter orientation of AlN would be expected on Si (111), as the closest-packed (0001) planes of AlN contain the same general atomic arrangement. Previous reports of AlN on Si(100) are inconsistent with regard to orientational relationships. Several researchers have used trimethyaluminum and NH_3 in CVD growth on on-axis Si(100) substrates. Morita et al. [13] deposited single-crystal AlN(0001) on Si(100) at 1260°C. Yu et al. [14] grew epitaxial AlN$(10\bar{1}0)$ on Si(100) at temperatures as low as 400°C. Roughening and pitting of the Si surface has been observed at temperatures as low as 800°C [24]. Thus, the roughness of the Si surface is likely to be more severe at 1260°C than at 400°C due to the evaporation of the oxide and the greater surface mobility at the higher temperature. This degradation of the surface may also explain why the films grown as a part of this study were AlN(0001) rather than AlN$(10\bar{1}0)$.

In summary, monocrystalline AlN films were grown on vicinal α(6H)-SiC(0001) at 1050-1200°C using thermally evaporated Al and ECR plasma decomposition of N_2. The surfaces of the films formed at 1200°C were rough. Films grown at 1050°C were much smoother and formed an abrupt interface with the substrate. These latter films were of excellent microstructural quality when compared to those grown by CVD and reported in the literature. Highly oriented AlN(0001) films with a very smooth surface morphology were also formed on vicinal Si(100) at 1050°C. This c-axis alignment is believed to be caused by the roughness and pitting in the Si surface at the elevated growth temperatures. Doping with candidate n- and p-type impurities and the determination of the resultant properties of the AlN films will be investigated in the near future.

ACKNOWLEDGEMENTS

The authors acknowledge the support of this research by the Office of Naval Research under Grant #N00014-90-J-1427. We also express our appreciation to Applied Science and Technology (ASTeX), Inc., Woburn, MA for the ECR source, to Cree Research, Inc., Durham, NC for the vicinal α(6H)-SiC substrates, and to Ms. S. Rogers for the Auger analysis.

REFERENCES

1. W. M. Yim, E. J. Stofko, P. J. Zanzucchi, J. I. Pankove, M. Ettenberg, and S. L. Gilbert, J. Appl. Phys. **44**, 292 (1973).
2. M. G. Norton, B. C. H. Steele, and C. A. Leach, *Science of Ceramics*, **14**, 545 (1988).
3. G. A. Slack, J. Phys. Chem. Solids **34**, 321 (1973).
4. M. Kitayama, T. Fukui, T. Shiosaki, and A. Kawabata, Japan J. Appl. Phys. **22**, 139 (1982).
5. G. R. Kline and K. M. Lakin, Proc. IEEE Symp. Ultrasonics **14**, 495 (1983).

6. K. Tsubouchi, K. Sugai, and N. Mikoshiba, Proc. IEEE Symp. Ultrasonics **14**, 340 (1983).
7 M. Sano and M. Aoki, Oyo Butsuri, **52**, 374 (1983).
8. J. K. Liu, K. M. Lakin, and K. L. Wang, J. Appl. Phys **46**, 3703 (1975).
9. M. Morita, N. Uesugi, S. Isogai, K. Tsubouchi, and N. Mikoshiba, Jpn. J. Appl. Phys. **20**, 17 (1981).
10. G. D. O'Clock, Jr. and M. T. Duffy, Appl. Phys. Lett. **23**, 55 (1973).
11. T. L. Chu, D. W. Ing, and A. J. Norieka, Solid State Electron. **10**, 1023 (1967).
12. H. M. Manasevit, F. M. Erdmann, and W. I. Simpson, J. Electrochem. Soc. **118**, 1864 (1971).
13. M. Morita, S. Isogai, N. Shimizu, K. Tsubouchi, and N. Mikoshiba, Japan. J. Appl. Phys. **20**, L173 (1981).
14. Z. J. Yu, J. H. Edgar, A. U. Ahmed, and A. Rys, J. Electrochem. Soc. **138**, 196 (1991).
15. A. J. Noreika and D. W. Ing, J. Appl. Phys. **19**, 5578 (1968).
16. S. Yoshida, S. Mizawa, Y. Fujii, S. Takada, H. Hayakawa, S. Gonda, and A. Itoh, J. Vac. Sci. Technol. **16**, 990 (1979).
17. Z. Sitar, M. J. Paisley, B. Yan, R. F. Davis, J. Ruan, and J. W. Choyke, Thin Solid Films **200**, 311 (1991).
18. L. B. Rowland, R. S. Kern, S. Tanaka, and R. F. Davis, in *Proceedings of the Fourth International Conference on Amorphous and Crystalline Silicon Carbide* (Springer-Verlag, Berlin), to be published.
19. S. Kaneda, Y. Sakamoto, C. Nishi, M. Kanaya, and S. Hannai, Japan. J. Appl. Phys. **25**, 1307 (1986).
20. T. Sugii, T. Aoyama, and T. Ito, J. Electrochem. Soc. **137**, 989 (1990).
21. L. B. Rowland, R. S. Kern, S. Tanaka, and R. F. Davis, submitted for publication.
22. T. Yoshinobu, H. Mitsui, I. Izumikawa, T. Fuyuki, and H. Matusnami, Appl. Phys. Lett. **60**, 824 (1992).
23. D. J. Robbins, A. J. Pidduck, A. G. Cullis, N. G. Chew, R. W. Hardeman, D. B. Gasson, C. Pickering, A. C. Daw, M. Johnson, and R. Jones, J. Cryst. Growth **81**, 421 (1987).

IV. Deposition of Pseudomorphic Layers of Intrinsic Undoped, Magnesium Doped p-type and Silicon Doped n-type GaN Films on AlN Films

A. Introduction

During last three decades, the growth and the characterization of GaN films have received considerable attention [1]. However, until recently, the application of this material in terms of devices was relegated to MIS light emitting diodes due to the unsuccessful deposition of p-type films. To date, the introduction during growth of acceptor-like dopants, such as Mg and Zn, resulted only in compensation. For example, the electrical properties of the GaN films changed from being highly conductive n-type, for the undoped film to highly resistive for the acceptor-doped films. However, recently a Japanese research group observed p-type character in a Mg-doped GaN film after a post-deposition Low-Energy Electron-Beam Irradiation (LEEBI) treatment [2]. However, to date there is no explanation for this phenomena. In order to make commercial devices, one should have the capability to activate the acceptor dopants in GaN during the growth and, thus, to make p-type GaN films directly.

In this report, we will show that direct deposition of p-type GaN films has been achieved. We have found that improving the crystalline quality of the deposited GaN film caused its electrical properties to change from a highly n-type material to one having a very high resistance. In our research, this was accomplished by preventing the formation of a thin amorphous interfacial layer on the SiC substrate and by growing a AlN buffer layer on both the SiC and the sapphire substrates. Furthermore, we have shown for the first time that as-deposited p-type GaN films can be produced using this deposition procedure.

The effect of Si doping has also been investigated. Only films deposited on sapphire have been doped due to the limited supply of α-SiC substrates. Preliminary results indicated that n-type GaN films were obtained by Si doping. The resistivity and carrier concentration of these films were $\approx 10^{-2}$ Ω·cm and $\sim 6\times10^{18}$ cm^{-3}, respectively.

B. Experimental Procedure

The deposition system employed in this research was a commercial Perkin-Elmer 430 MBE system. This system consists of three parts: a load lock (base pressure of 5×10^{-8} Torr), a transfer tube (base pressure of 1×10^{-10} Torr), which also was used for degas the substrates, and the growth chamber (base pressure of 5×10^{-11} Torr). Knudson effusion cells with BN crucibles and Ta wire heaters were charged with 7N pure Gallium, 6N pure aluminum, 6N pure magnesium and 6N pure silicon respectively. Ultra-high purity nitrogen, further purified by a chemical purifier, was used as the sources gas. And it was excited by an ECR plasma source, which was designed to fit inside the 2.25 inch diameter tube of the source flange cryoshroud. The details of the system can be found elsewhere [3].

The substrates were (0001) oriented α(6H)-SiC and epitaxial quality sapphire wafers. Prior to loading into the chamber, the α-SiC substrates were cleaned by a standard degreasing and RCA cleaning procedure. The sapphire substrates were cleaned using the following procedure: degreasing and DI water rinse, 10 minutes in a hot solution of HPO_3:H_2SO_4 with 1:1 ratio, DI water rinse, finally dip in 1:10 solution of 49% HF:H_2O. All substrates were mounted on a 3-inch molybdenum block and loaded into the system. After undergoing a degassing procedure (700°C for 30 minutes), the substrates were transferred into the deposition chamber. Finally RHEED was performed to examine the crystalline quality of the surfaces of the substrates.

C. Results

Deposition of high quality undoped GaN films. In the past, single crystal GaN films have been successfully deposited on a variety of substrates using the NCSU modified gas source MBE system. However, the resistivity of those as-deposited films was low, and they exhibited an n-type character. We have also found for the films deposited on α-SiC (0001) substrates, a thin amorphous silicon nitride layer existed at the interface of substrates and the deposited GaN films [4]. This resulted from the interaction of activate nitrogen species produced in the ECR plasma source with the SiC surface prior to opening the Ga or Al shutter at the outset of the deposition. The RHEED pattern of both the α-SiC and sapphire substrates changed after exposure to the nitrogen plasma. We found that this change could occur for exposure to the nitrogen plasma for times as little as five minutes.

We have developed the following technique to prevent this amorphous interfacial layer from forming on the substrate surface. The procedure involves an initial exposure of the substrate to pure Al followed by the exposure of this Al to reactive N. During this time, these Al layers reacted with the plasma activated nitrogen species and formed an AlN layer. The details of re-acting metal Al with activated N_2 species to form AlN can be found in a report by J. A. Taylor [5]. The film growth was subsequently initiated using the deposition conditions listed in the Table I.

Table I. Deposition Conditions for Undoped GaN Films

Nitrogen pressure	2×10^{-4} Torr
Microwave power	50W
Gallium cell temperature	990°C
Aluminum cell temperature	1120°C
substrate temperature	650°C
Al layer	2 monatomic layer
AlN buffer layer	150~200Å
GaN	4000~5000Å

An AlN buffer layer having a thickness of about 150Å was used to reduce the lattice mismatch between the substrate and GaN [6]. Reflection High Energy Electron Diffraction (RHEED) and SEM were performed to examine the quality of the deposited GaN films. RHEED patterns taken on the <2$\bar{1}\bar{1}$0> azimuth of GaN films deposited on (0001)-oriented α-SiC and sapphire substrates are shown in Figure 1. An analysis of these RHEED patterns indicated that both the AlN buffer layer and the GaN film are monocrystalline films. The RHEED pattern of the final surface of the GaN films indicated that they possessed reasonable crystalline quality and a smooth surface. Kikuchi lines were observed on the RHEED screen, but can not be photographed due to the low contrast. A spotty RHEED pattern was obtained for the GaN film deposited on the sapphire substrate due to sample charging of the resistive film. This is also discussed below. The surface morphology of the films was also examined by SEM. The featureless picture, shown in Figure 2, is indicative of the smooth surface of the deposited GaN film and agreed well with the RHEED pattern results.

Deposition of Mg-doped GaN films. Based on above results, we investigated the incorporation of the acceptor dopant, Mg, into the films. The deposition conditions for Mg-doped GaN films were same as that for undoped GaN films described before, except that a Mg-source was used in the deposition. Table II lists the typical deposition conditions for Mg-doped GaN films.

Table II. Deposition Conditions for Mg-doped GaN Films

Nitrogen pressure	2×10^{-4} Torr
Microwave power	50W
Gallium cell temperature	990°C
Aluminum cell temperature	1120°C
Magnesium cell temperature	~300°C
substrate temperature	650°C
Al layer	2 monatomic layer
AlN buffer layer	150~200Å
Mg-doped GaN	4000~5000Å

(a)

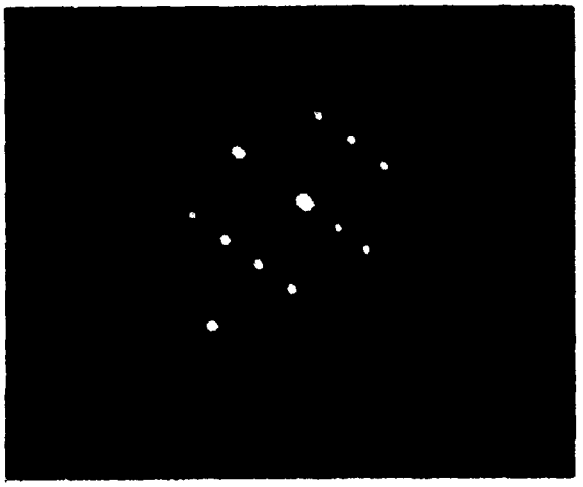

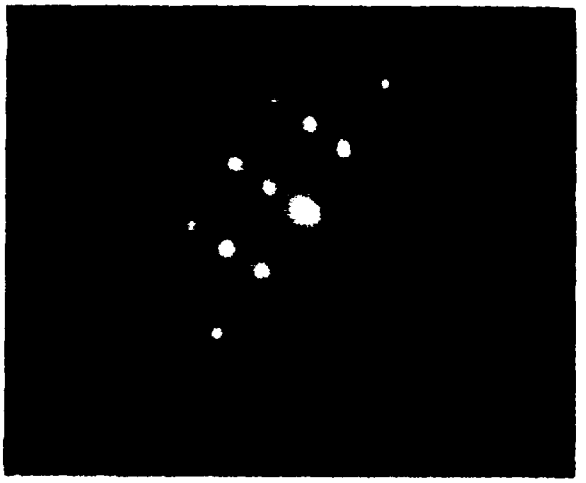

(b) (c)

Figure 1. RHEED patterns taken in the <2TT0> azimuth of a) AlN buffer layer on α-SiC substrate, b) GaN film on AlN/α-SiC substrate, c) GaN film on AlN/sapphire substrate.

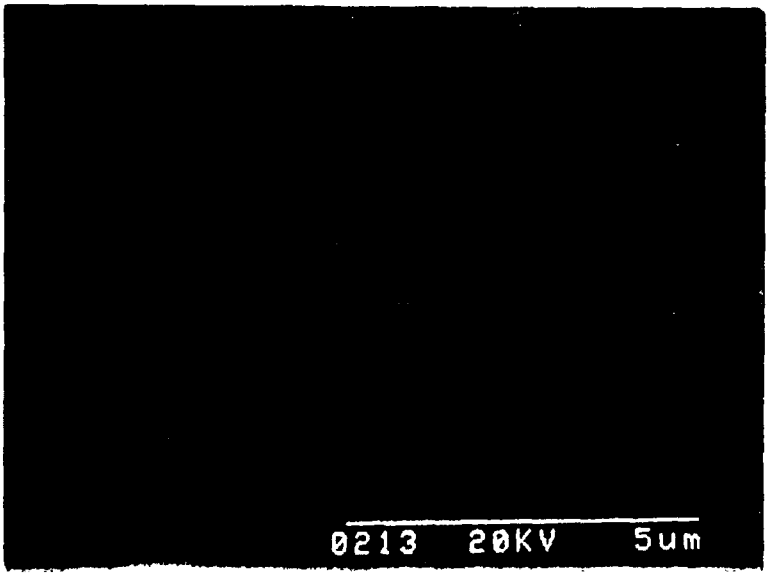

Figure 2. SEM photograph of the surface of an undoped GaN film deposited on a AlN/α-SiC substrate.

The RHEED patterns of the Mg-doped films also showed features indicative of good crystalline quality. The representative SEM picture in Figure 3 shows that the Mg-doped GaN film also had a very smooth surface.

Electrical properties of undoped and Mg-doped GaN films. The electrical properties of the films have been characterized using the van der Pauw resistivity measurement technique and Hall effect measurements. Indium was used as the electrical contacts. Current-voltage (IV) measurements were first performed to check the contact character. As shown in Fig. 4(a), the undoped GaN film was quite resistive; a non-ohmic IV character was observed after a voltage larger than 15 volts was applied. The Mg-doped GaN films was much more conductive, as shown in Fig. 4(b), and IV measurements of the contacts indicated ohmic character. It is clear from this point that eliminating the amorphous interfacial layer at the substrate surface results in a dramatic improvement in the electrical properties. The early work conducted in our research group showed that even Mg-doped GaN made at that time possessed a non-ohmic IV character similar to that of the undoped GaN films made in this reporting period [7]. Resistivity and Hall effect measurements were performed for both undoped and Mg-doped GaN films. The results were summarized in the Table III. Note that for the undoped GaN films, the highly resistive character made the electrical measurements very difficult. By contrast, for the Mg-doped GaN films, a p-type conductive character was identified, and the measured electrical properties were similar to those recently reported for the low-energy electron-beam irradiation (LEEBI) treated Mg-doped GaN film [2,8]. Furthermore, the p-type conductive character of the Mg-doped films were also identified by the thermal-probe method.

Table III. Electrical Properties of Undoped and Mg-doped GaN Films

films	undoped GaN	Mg-doped GaN
resistivity (Ω·cm)	$>10^2$	0.3
conductive type	x	P-type
mobility ($cm^2/V·s$)	?	~10
carrier concentration (cm^{-3})	$<10^{16}$	$\sim 1\times10^{18}$

Figure 3. SEM photograph of the surface of the undoped GaN film deposited on an AlN/α-SiC substrate.

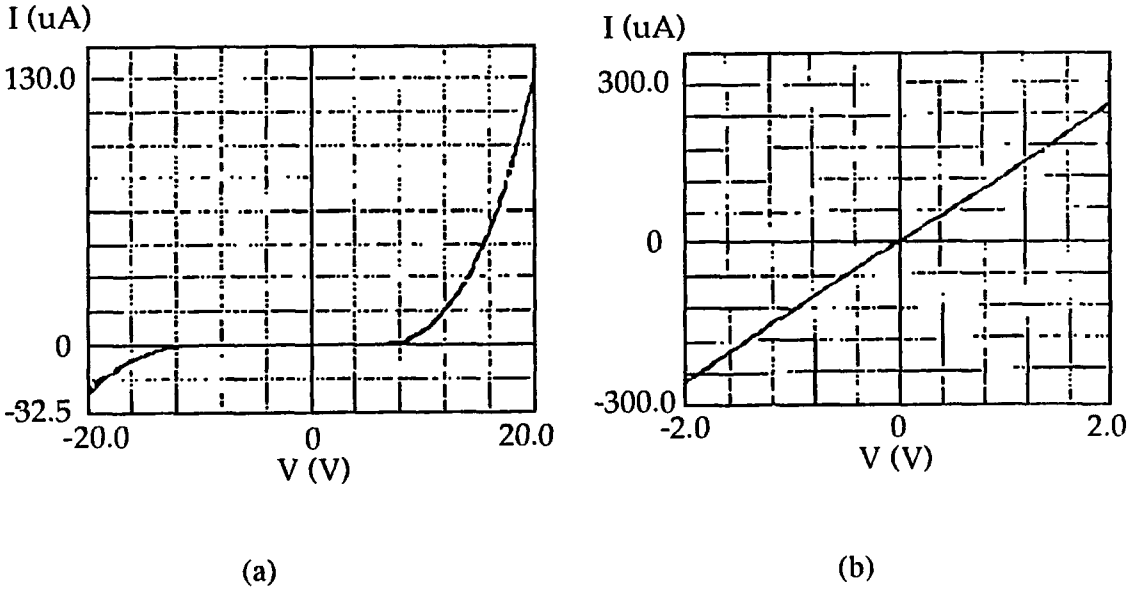

(a) (b)

Figure 4. IV Curves for (a) an undoped GaN film, (b) a Mg-doped GaN film.

The temperature dependence of the resistivity for a p-type Mg-doped GaN film has also been measured. The results are shown in Figure 5. The resistivity decreased with increasing temperature due to the increasing ionization of the Mg acceptors.

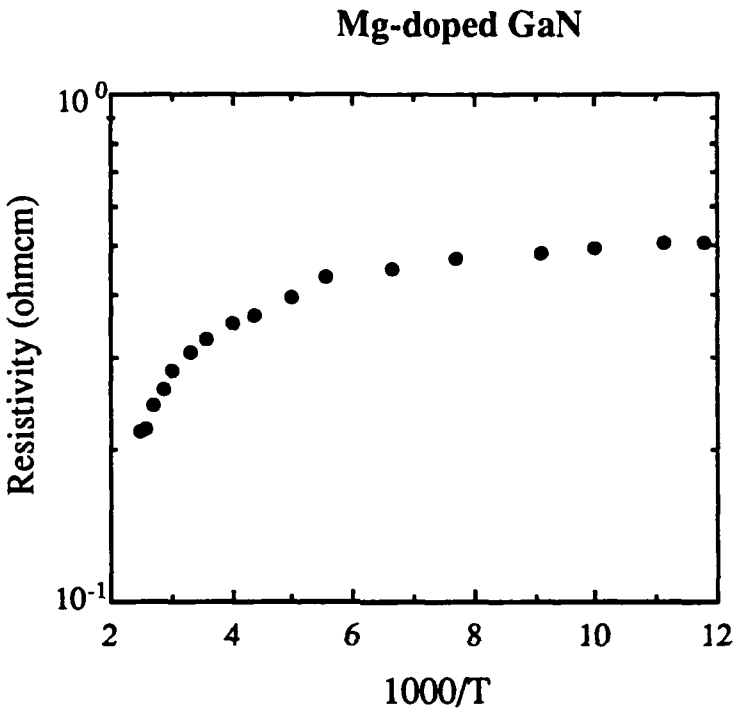

Figure 5. Temperature dependence of resistivity for a Mg-doped p-type GaN film.

Growth of Si-doped GaN films on (0001) sapphire substrates. Based on the results that undoped GaN films were highly resistive, we have investigated the incorporation of the donor-like dopant, Si, into the films to obtain n-type GaN films. The Si-doping process was accomplished in the same manner as the Mg-doping described above. The deposition conditions for producing Si-doped GaN films were the same as that for undoped GaN films, but with the use of the Si-source. This study has been conducted only on the films deposited on (0001) sapphire substrates due to the limited supply of α-SiC substrates. Table IV lists the typical deposition conditions employed to produce these films.

The Si-concentration in the films was varied by controlling the Si-cell temperature. RHEED patterns of the Si-doped films indicated that the film structure changed with an increase in the temperature of the Si-cell. Polycrystalline RHEED patterns occurred for the films deposited with Si-cell temperatures exceeding 1180°C.

Table IV. Deposition Conditions for Si-doped GaN Films

Nitrogen pressure	2×10^{-4} Torr
Microwave power	50W
Gallium cell temperature	990°C
Aluminum cell temperature	1120°C
Silicon cell temperature	900~1300°C
substrate temperature	650°C
Al layer	2 monatomic layers
AlN buffer layer	150~200Å
Si-doped GaN	4000~5000Å

The effect of Si doping on the electrical properties of GaN films was again investigated using the van der Pauw resistivity measurement and Hall effect measurements. It was found that GaN films deposited with the Si-cell temperature lower than 1180°C, were still very resistive. When the Si-cell temperatures reached 1200°C or higher, doped GaN films became very conductive, with a resistivity of $10^{-1}\Omega\cdot$cm or less. However, each of these films showed a polycrystalline RHEED pattern. The maximum Si-cell temperature at which doped GaN films still showed a single crystal RHEED pattern was 1180°C.

The atomic Si-concentration in the films was characterized by SIMS measurements and compared to the free carrier concentration determined by Hall effect measurements. It was found that generally in these Si-doped GaN films, as shown in Figure 6. The atomic Si composition was about two orders higher than the free carrier concentration. This large concentration of inactive Si atoms leads to the degradation of the crystal quality of the film resulting finally in the formation of polycrystalline material. We subsequently limited the temperature of the Si-cell to 1180°C. The typical electrical properties of the Si-doped GaN films are listed in the Table V.

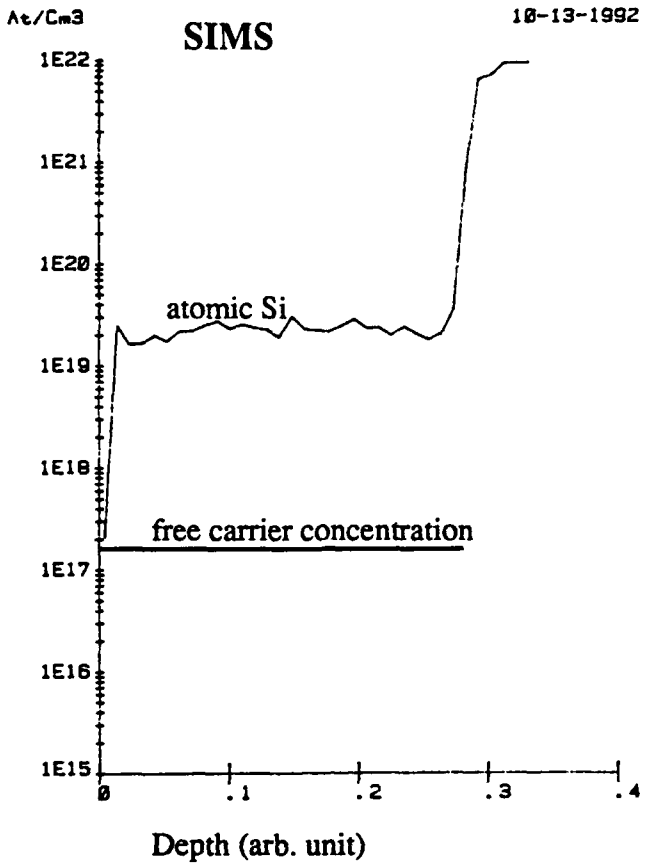

Figure 6. SIMS profile for the Si doped GaN film deposited at the Si-cell temperature of 1180°C.

Table V. Electrical Properties of Undoped and Si-doped GaN Films

	Si-doped GaN
Si-cell temperature	1180°C
conductive type	N
resistivity (Ω·Πcm)	31
carrier concentration (cm^{-3})	1.7×10^{17}
atomic Si concentration (cm^{-3})	2×10^{19}

As indicated above, a certain concentration of the atomic Si in the films was electrically inactive. To further activate these atomic Si, the deposition temperature was increased. The results shown in Table VI indicate that with increasing deposition temperature to 950°C, the

deposited films became more conductive. The resistivity decreased to 0.02Ω·cm, and the free carrier concentrations increased to 5.6×10^{18}cm^{-3}. However with a further increase in deposition temperature above 1050°C, the films again became resistive. RHEED measurements indicated that the films deposited at temperature of 1000°C or higher had very rough surfaces. Another problem also occurred at high deposition temperature, namely, the sample surfaces were contaminated by the silver paste mounting material.

Table VI. Effect of Deposition Temperature on Electrical Properties of Si-doped GaN Films

deposition temperature	resistivity (Ω·cm)	carrier concentration (cm^{-3})
650	10.6	1.7×10^{17}
850	0.14	4.3×10^{18}
950	0.02	5.6×10^{18}
1050	too resistive	?

We have also investigated another way to activate the excess atomic Si. In this approach the growth surface was exposed to a UV lamp during deposition, while keeping the substrate temperature at 650°C. The lamp was a 500W mercury arc lamp that was installed in front of a sapphire view port in the center of the source flange and oriented normal to the substrate. The illumination intensity at the growth surface was estimated at about 0.4 W/cm^2 [8]. Preliminary studies have shown that under the same deposition conditions, the resistivities decreased from 10.6 Ω·cm for a film deposited without the lamp illumination to about 0.03 Ω·cm for a film deposited with the lamp illumination; the free carrier concentration increased from 1.7×10^{17} cm^{-3} to about 3.7×10^{18} cm^{-3}.

Electron Microscopy Characterization of Films. The microstructures of the films discussed in this report were further characterized by scanning electron microscopy (SEM) and transmission electron microscopy (TEM). SEM was performed in a Hitachi S-800 SEM with a field emission gun. The samples were coated with a thin conductive layer of carbon to avoid charging effects. Carbon was deposited on a different area of the sample than that used for preparation of TEM samples. Unless otherwise noted, TEM was performed in a JEOL 4000EX operated at 400kV. High Resolution images were recorded using a 1mr convergence semi-angle at Scherzer defocus (~ -47nm). Cross-sectional transmission electron microscopy (XTEM) samples were prepared using standard techniques.

As described earlier, high quality undoped GaN films have been achieved by eliminating the interfacial amorphous layer. The small dimensional features in the surface morphology in the SEM image of the film deposited with the AlN buffer layer, shown in Figure 7, indicated a smooth surface of the deposited GaN film and agreed well with the RHEED pattern results. However, high resolution TEM results revealed the films, deposited on both α-SiC and sapphire substrates, had a columnar structure, as shown in Figure 8, although the RHEED patterns indicated single crystal material. This contradiction is due to the very high degree of preferred orientation of the columns. The defects creating the columnar structure appear to originate at the AlN/SiC interface; however, they increase in number at the GaN/AlN interface. TEM also revealed a rough interface between the AlN and GaN layers, as shown in Figure 8.

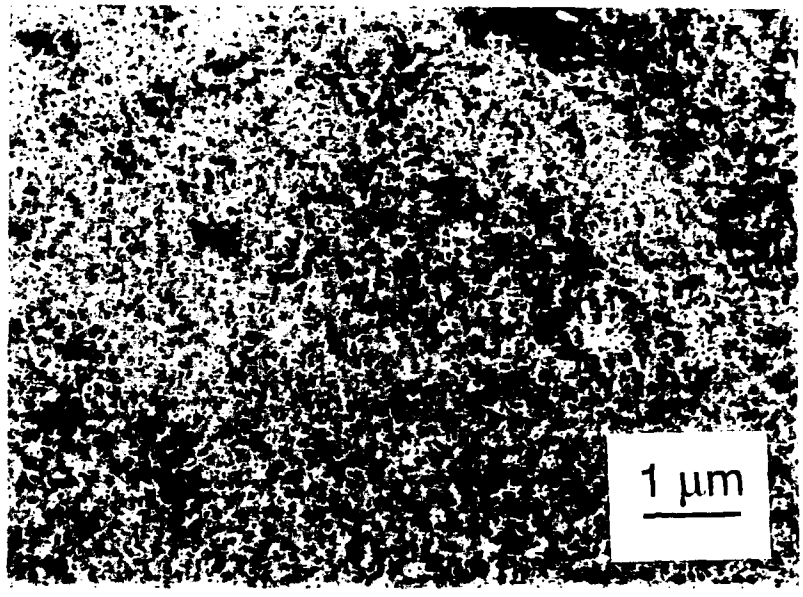

Figure 7. SEM micrograph of the undoped GaN film.

The growth of high quality, single crystal films of AlN has been achieved on α-SiC substrates at higher deposition temperatures (~1100°C) in other research in our group [9]. Therefore, in an attempt to eliminate the columnar structure, we have deposited the thin AlN buffer layer at a higher temperature (1100°C), followed by the deposition of GaN at 650°C. The SEM analysis showed very small surface features; although, XTEM revealed that the film again consisted of a columnar structure. No apparent improvement was gained from the increase in deposition temperature of the buffer layer.

Because there was an increase in the number of defects at the GaN/AlN interface, the effects of the deposition of GaN films on α-SiC substrates without the aide of a buffer layer was investigated at 650° C. A columnar morphology was also observed. It was initiated at the

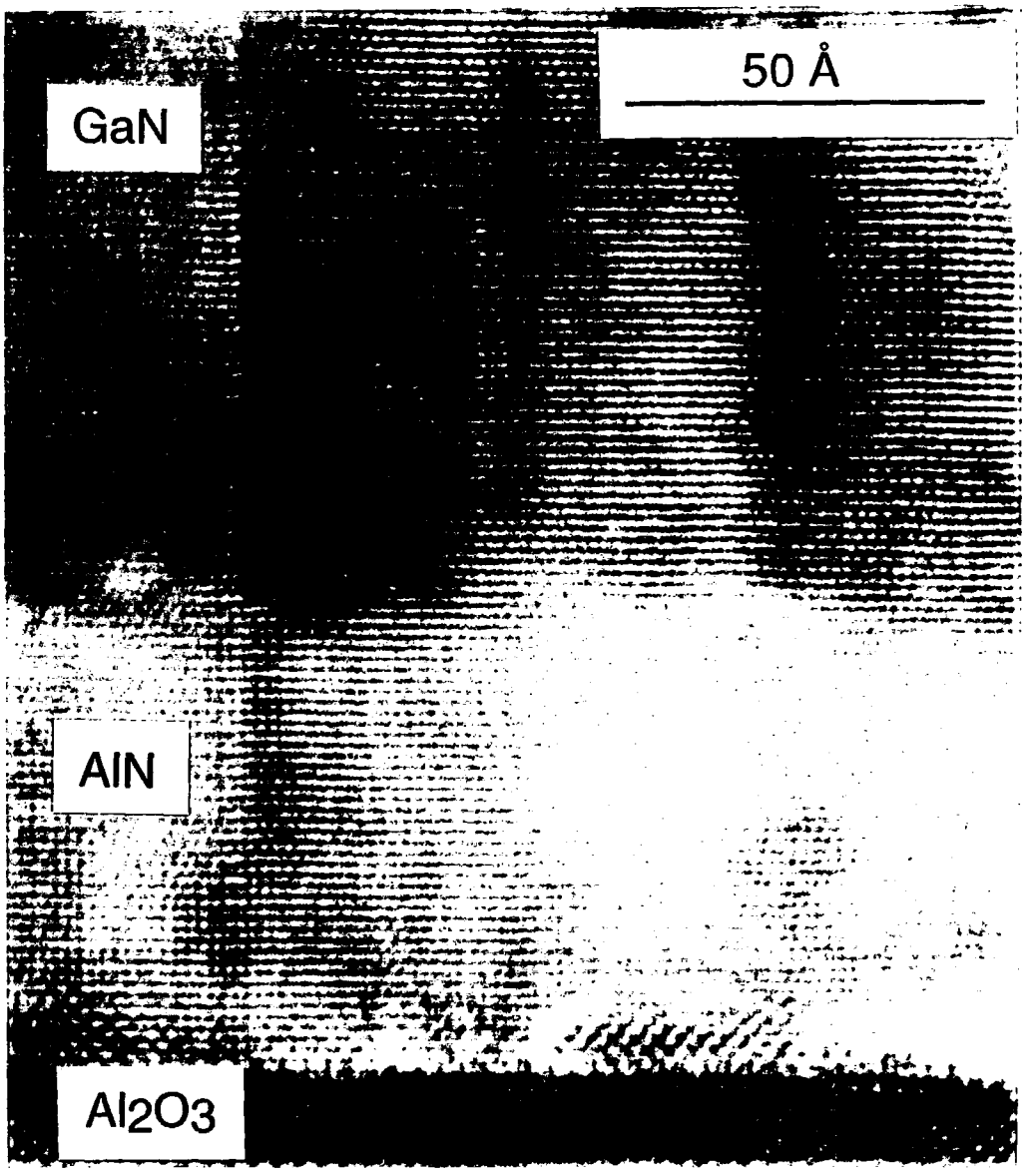

Figure 8(a). TEM micrograph of the undoped GaN films on (a) sapphire (microscopy performed on a Topcon 002B).

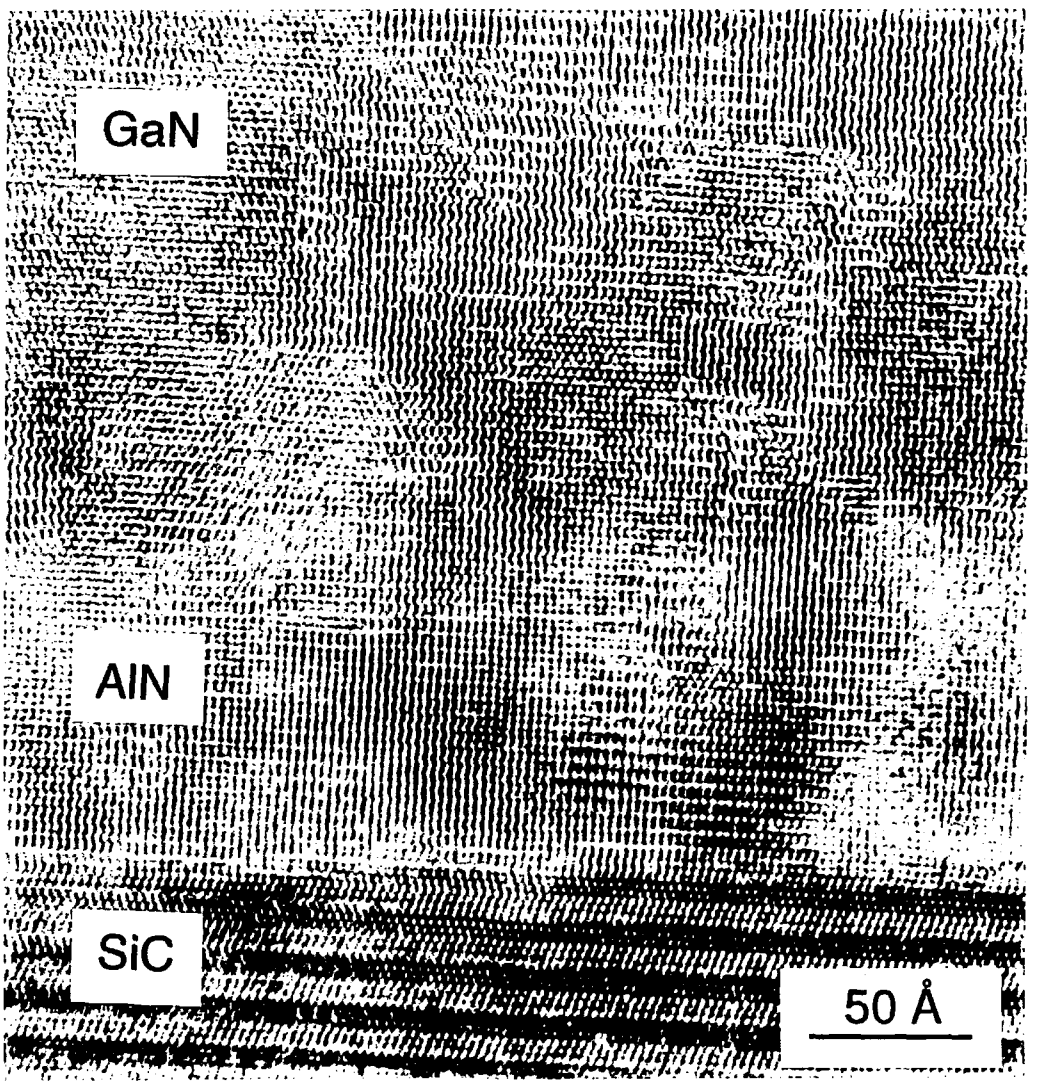

Figure 8(b). TEM micrograph of the undoped GaN films on (b) α-SiC substrates.

SiC/GaN interface. The cause of the columnar structure is possibly the lattice mismatch between the GaN and the α-SiC substrate.

Though AlN has been used as a buffer layer between GaN and the substrates by most research groups, there is still a 2.4% lattice mismatch at the GaN/AlN interface, which could cause the formation of the columnar structure. To avoid this lattice mismatch, we attempted the deposition of a compositionally graded buffer layer subsequent to the growth of the pure AlN film. The goal was to continuously change the composition of this layer from pure AlN to pure GaN. This layer was followed by the deposition of a GaN film. The SEM micrograph of this film, shown in Figure 9, reveals a rough surface which is indicative of a polycrystalline material. XTEM analysis confirmed the polycrystalline nature of the film, as shown in Figure 10. Selected area diffraction (SAD) reveals that the GaN is first deposited in the wurtzite structure but converts to a cubic structure as deposition is continued. This is very likely due to the action of the numerous stacking faults. This micrograph also shows that there was an abrupt change from the AlN to the GaN instead of a gradually graded layer. This is very likely caused by the much stronger attraction of Al to N than the attraction of Ga to N. Further research will attempt to improve the deposition of the graded layer.

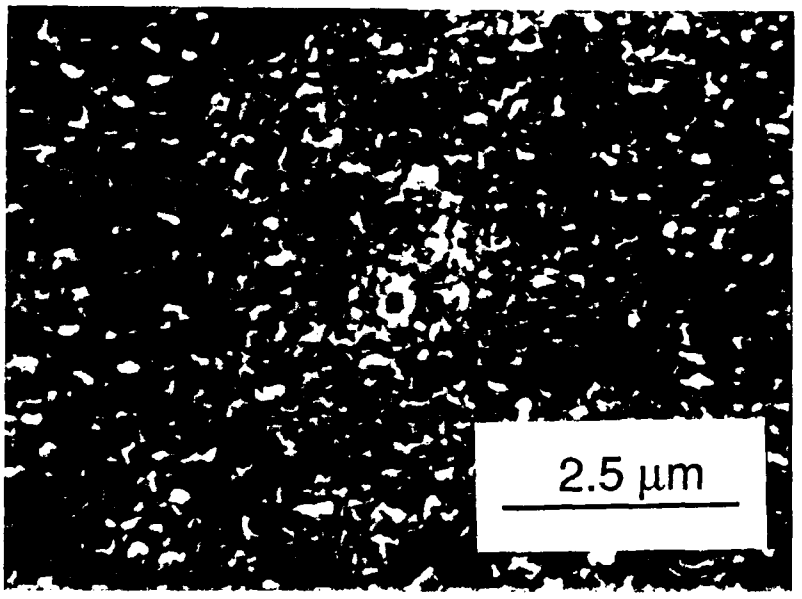

Figure 9. SEM image of an undoped GaN film deposited with a graded $Al_xGa_{1-x}N$ layer.

By comparison to chemical vapor deposition (CVD) in which the growth temperature for GaN films is as high as 1200°C, our modified gas source MBE technique employs a much lower deposition temperature (650°C). Subsequent growth examined the effects of depositing both the buffer layer and the GaN film at higher temperatures (1100°C). XTEM analysis

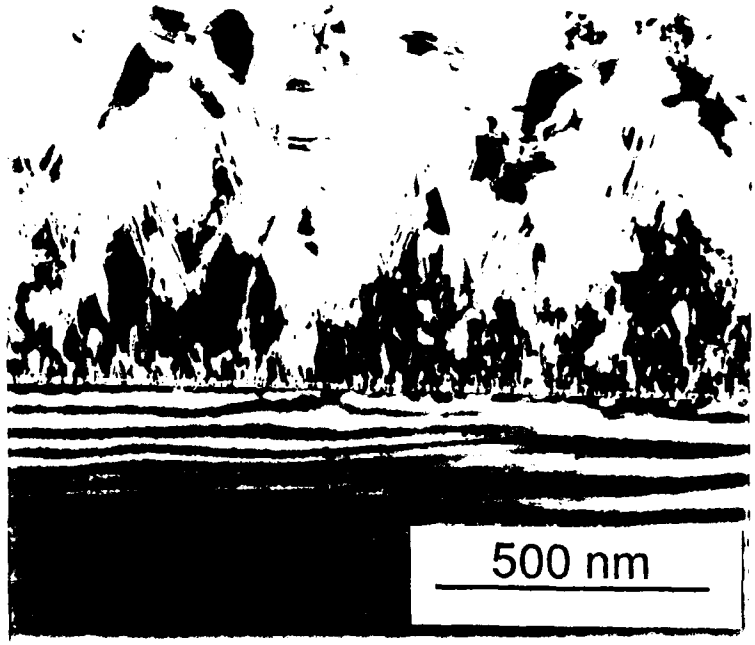

Figure 10. TEM micrograph of an undoped GaN film with a graded $Al_xGa_{1-x}N$ layer.

revealed that the GaN portion of the film was no longer continuous. From these preliminary results, it is tentatively believed that the plasma may be etching the growth surface as the film is being deposited, particularly at these high temperatures. This would create a rough surface in which defects easily form and a columnar structure results. Further investigation is needed to study the effects of ECR plasma source on the structure of deposited films. It may also be that at the much lower beam pressures used in MBE (10^{-4}–10^{-5} Torr) relative to CVD (1 atm), the GaN is unstable to thermal evaporation.

D. Discussion

Undoped GaN films, made by different groups or by different deposition techniques, have been almost universally reported to be conductive and to exhibit n-type conductive character. By contrast, as-deposited Mg-doped GaN films resulted only in being compensated and were very resistive. No as-deposited p-type GaN films had been reported, though a Japanese research group had reported that p-type conductive character is observed on Mg-doped GaN films exposed to post-deposition low-energy electron-beam irradiation [2]. Thus, the question is raised as to why p-type GaN films can not be deposited directly. Moreover, what prohibits the activation of an acceptor dopant? Finally, is the LEEBI treatment the only way to produce p-type GaN films and, if so, why? Answers for these are far from clear yet at this time.

Recently S. Nakamura et. al. postulated from experimental evidence that the acceptor (e.g. Mg)-H neutral complexes formed in as-deposited Mg-doped GaN films and were responsible

for the unsuccessful p-type doping. In addition, these complexes were decomposed by a low-energy electron-beam irradiation treatment. This resulted in the activation of the acceptor dopant and the achievement of p-type doping [10]. However, as yet they have provided no chemical evidence for the existence of hydrogen in their GaN films. We believe that the deactivation of the acceptor dopants in the GaN films may also be related to the existence of a large density of defects, which could trap these dopants. Some of the dopant atoms may be weakly bonded to these defects. The LEEBI treatment, breaks these weak bonds and results in the activation of the acceptor dopants.

Our research group has shown previously [7] that, even under the best deposition conditions, undoped GaN films were still conductive and n-type while Mg-doped GaN films were very resistive. Some changes were also observed after our LEEBI treatment, but they were not as dramatic as the Japanese have reported. In contrast to these early research results, our recent work has shown that by eliminating the amorphous interfacial layer between the substrates and the deposited films, the crystalline quality of the deposited GaN film can be greatly improved. In this way, deposited undoped GaN films become intrinsic, while Mg-doped GaN films become p-type films. This is the further evidence that unsuccessful p-type doping in prior research in other laboratories was mainly due to the existence of electrically activated micro-structural defects in the deposited films.

It also should be pointed out that although as-deposited p-type GaN films can be produced, the hole mobility is quite low. Thus, is low hole mobility an intrinsic property of GaN films or is it caused by their poor microstructural quality? It is well known that the lack of lattice matched substrate materials for GaN make heteroepitaxy quite difficult. A large amount of lattice mismatch still exists even when AlN is used as a buffer layer. We believe that micro-structural defects related to the lattice mismatch can be further reduced if we can find the "right" substrates, such as using a graded $Al_xGa_{1-x}N$ solid solution as a buffer layer. Furthermore, from our high resolution TEM work presented in this report, we have found that the undoped GaN films possess the columnar structure, and the columnar structure definitely contains a high density of defects which may be the cause of the low carrier mobility. No other researchers have presented TEM data that is necessary to determine the effects of columnar structure on possible device fabrication.

E. Conclusions

We have shown that in the use of our modified gas source MBE system, a thin amorphous layer was formed on the surfaces of the SiC and sapphire substrates during exposure to the nitrogen plasma prior to the deposition of the AlN or GaN films. This was prevented by exposing the substrate to an Al or Ga flux sufficient to deposit a submonolayer of metal prior to starting the nitrogen plasma. As a result, the undoped GaN films showed intrinsic electrical

character and were very resistive. Furthermore, by in-situ incorporation of Mg into the films, as-deposited, p-type GaN films were produced for the first time. These latter films had a resistivity = 0.5 Ω·cm, a Hall mobility = 10 $cm^2/V \cdot s$ and a carrier concentration of 1×10^{18} cm^{-3}, respectively. Si-doped n-type GaN films have also been achieved.

F. Future Research Plans

As noted in the Discussion Section of this report, a graded $Al_xGa_{1-x}N$ solid solution may also be chosen as the buffer layer for the homoepitaxy of GaN. Therefore, some of our future efforts will involve the growth of a good quality graded $Al_xGa_{1-x}N$ solid solution buffer layer. The purpose of this study will be to improve the microstructure and carrier mobility of the deposited GaN. The growth of n- and p-type GaN films will be further investigated. Also the cause of the columnar structure in the films will be further investigated and eliminated.

G. References

1. R. F. Davis, "Current Status of the Research on III-V Mononitrides Thin Films for Electronic and Optoelectronic Applications," in The *Physics and Chemistry of Carbides, Nitrides and Borides*, R. Freer, ed. Kluwer Academic Publishers, Dordrecht, The Netherlands, 1990, pp. 653-669.
2. H. Amano, M. Kito, K. Hiramatsu and I. Akasaki, Jap. J. Appl. Phys. **28**, l2112 (1989).
3. Z. Sitar, M. J. Paisley, D. K. Smith and R. F. Davis, "Design and Performance of an Electron Cyclotron Resonance Plasma Source for Standard Molecular Beam Epitaxy Equipment," Rev. Sci. Instrum. **61**, 2407 (1990).
4. Z. Sitar, L. L. Smith and R. F. Davis, "Morphology and Interface Chemistry of the Initial Growth of GaN and AlN on a-SiC and Sapphire," MRS Symp. Proc. **237**, 583 (1991).
5. J. A. Taylor and J. W. Rabalais, "Reaction of $N2^+$ beam with Aluminum Surfaces," J. Chem. Phys. **75**, 1375 (1981).
6. S. Yoshida, S. Misawa and S. Gonda, "Improvements on the Electrical and Luminescent Properties os Reactive Molecular Beam Epitaxy Grown GaN Films by Using AlN-coated Sapphire Substrates," Appl. Phys. Lett. **42**, 427 (1983).
7. R. F. Davis et. al., "The Effect of Electron Beam Irradiation on Mg Doped GaN Thin Films" in Final Technique Report N00014-86-K-0686 P5, 35 (1992).
8. M. Paisley, Ph.D. Thesis, 1992, NCSU, Raleigh
9. L. Rowland, Ph.D. Thesis, 1992, NCSU, Raleigh.
10. S. Nakamura, N. Iwas, M. Senoh and T. Mukai, "Hole Compensation Mechanism of p-type GaN Films," Jpn. J. Appl. Phys. **31**, 107 (1992).

V. Cubic Boron Nitride Thin Film Growth

A. Introduction

Cubic boron nitride is a material with potential applications due to both its tribological and electronic properties. It is the hardest material other than diamond, and it is more stable than diamond at higher temperatures. It does not react with the ferrous metals, which makes it an ideal cutting tool material. For electronic applications, it is of interest because it is a wide band gap (E_g=6.4 eV) semiconductor with very high thermal conductivity; yet it also has the potential of being doped as both a p-type and n-type semiconductor. Boron nitride is similar to carbon in having three basic structures, a layered hexagonal structure (h-BN) corresponding to graphite, a cubic structure (c-BN) corresponding to diamond, and a rare hexagonal wurtzite structure (w-BN) which corresponds to Lonsdaleite. The layered hexagonal structure is typically referred to simply as hexagonal BN. There are also variations of these structures, including turbostratic BN (t-BN), which, like hexagonal BN, consists of layers, but in which the layers are randomly oriented to each other [1].

Bulk cubic boron nitride was first synthesized in 1956 using high pressure-high temperature methods [2]. In recent years, cubic boron nitride has been grown in thin film form, using both chemical vapor deposition (CVD) and physical vapor deposition (PVD) methods [3-7].

In this work we are studying the growth of cubic boron nitride thin films, and attempting to grow films which could be used for electronic applications. We have studied the evolution of the films as they grow, and found that the phase of the films changes during growth. On Si substrates an initial amorphous BN layer forms, followed by a hexagonal BN layer, followed by growth of the cubic phase. These results have been written up and submitted to the Journal of Materials Research. A preprint of this article is included as Section VI.

We are also studying how the films grow on various substrates. In addition to growing the films on Si substrates, we have grown them on both single crystal diamonds and on diamond thin films. We have also used the c-BN films grown on Si substrates as substrates for diamond growth.

B. Experimental Procedure

Film Growth

A UHV ion beam assisted deposition (IBAD) system is being used for film deposition. Samples are loaded through a load lock system. Base pressures in the chamber are typically $< 1\times10^{-9}$ Torr. Boron is deposited by evaporating boron metal using an electron beam evaporator. Simultaneously a Kaufman type ion gun is used to bombard the depositing boron with both nitrogen and argon ions. The films are deposited onto heated substrates. A

schematic of the setup is shown in Figure 1. The deposition rate of the boron, the energy and flux of the ions, the ratio of the argon to nitrogen, and the substrate temperature can all be measured, controlled, and varied. The boron is evaporated using a Thermionics HM2 electron gun with an electromagnetic beam sweep. The boron sits in a graphite crucible liner which is in a water cooled 10 cc crucible. It is deposited at a rate of from 0.25 to 1.0 Å/s. The deposition rate is monitored using a quartz crystal monitor.

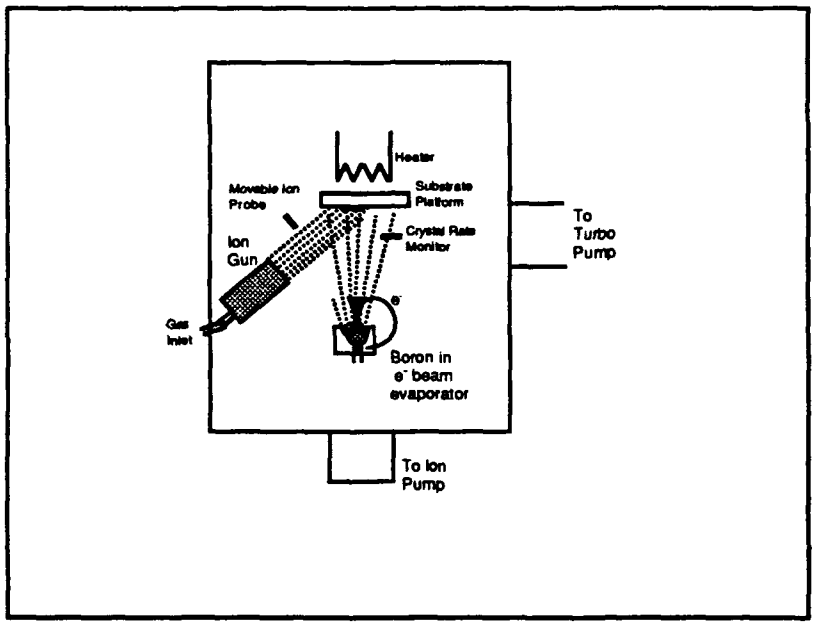

Figure 1. Schematic of deposition system.

The film is bombarded using an Ion Tech 3 cm Kaufman ion source. Bombardment is by nitrogen and argon ions in varied ratios, all at 500 eV. The flux of ions ranges from 0.05 to .30 mA/cm^2 and is measured using a negatively biased ion probe. The gas flow to the ion gun is 1.5 sccm for each of the two gases and is controlled using MKS mass flow controllers. Typical deposition pressures in the chamber are 1.0×10^{-4} Torr.

Substrates are heated from 300 to 700°C. The substrates used are 100 silicon wafers with high resistivity (25-45 W-cm) so as to be transparent for IR spectroscopy. Film thicknesses range from 100Å to 2000Å.

Film Characterization

FTIR. Fourier transform infrared spectroscopy (FTIR) has been found to be a convenient and reliable method for the purpose of determining whether a deposited film is cubic or hexagonal boron nitride. With FTIR analysis the cubic and hexagonal forms of boron nitride give distinct, independent peaks, due to the sp^3 and sp^2 bonds, respectively. Hexagonal boron

nitride has absorption peaks at 1367 cm^{-1} and at 783 cm^{-1} [8], while cubic boron nitride has a transverse optical mode absorption peak at 1075 cm^{-1} [9].

Transmission FTIR was carried out on an Analect Instruments model fx-6260 spectrometer. Transmission spectra were taken through the BN films and Si substrates. A spectra of an uncoated Si wafer was taken as a background scan, and the spectra of the coated wafer was ratioed against it. The Si wafers used as substrates were high resistivity wafers, >50 Ω cm, so as to transmit the IR radiation.

Reflectance FTIR was performed on films coated on substrates which are opaque to IR radiation, specifically Ni and Cu. This work was done on a Nicolet 620 FTIR with a Spectra Tech IR Plan optical microscope.

Electron microscopy. Structural characterization was accomplished by scanning electron microscopy (SEM) and transmission electron microscopy (TEM). SEM was performed in an Hitachi S-800 with a field emission gun. The samples were coated with a thin conductive layer of carbon to avoid charging effects. Carbon was deposited on a different area of the sample than that used for preparation of TEM samples. TEM was performed in a TOPCON EM-002B operated at 200 kV and a JEOL 4000EX operated at 400kV. On the JEOL microscope, high resolution images were recorded using a 1mr convergence semi-angle at Scherzer defocus (~ -47nm). Cross-sectional transmission electron microscopy (XTEM) samples were prepared using standard techniques [10].

XPS. X-ray photoelectron spectroscopy (XPS) was used to study the films. A Riber system, consisting of a Mac2 semi-dispersive electron energy analyzer and accessible by UHV transfer from the deposition chamber, was used. A Mg anode was used at 1.2 eV resolution for obtaining valence structure and 0.8 eV resolution for core level data.

Rutherford Backscattering. The stoichiometry of the films was measured using Rutherford backscattering (RBS), in which helium nuclei are used to bombard the film. By measuring the energy and angle of the backscattered nuclei, information about the film composition can be determined. RBS is particularly useful in that it gives a depth profile of the film, not only information about the surface layer.

C. Results

BN on single crystal diamond

Boron nitride was deposited on single crystal diamond. The diamond was natural diamond which had been cut and polished into substrates, obtained from Dubbledee company. Before loading, the diamonds were etched in a boiling H_2SO_4:HNO_3:$HClO_4$ solution in a ratio of 3:4:1 for 45 minutes to remove any graphitic phase. 1000 Å of BN was grown on the diamond, at substrate temperatures of 400° and 600°C. The FTIR patterns of the films are shown in Figure 2. A sharp c-BN peak is observed at ~1080 cm^{-1}. The h-BN peak is very

small. This spectra has a sharper c-BN peak, and a better c-BN to h-BN ratio than any films we had previously deposited on Si, and is as good or better than any that have appeared in the literature.

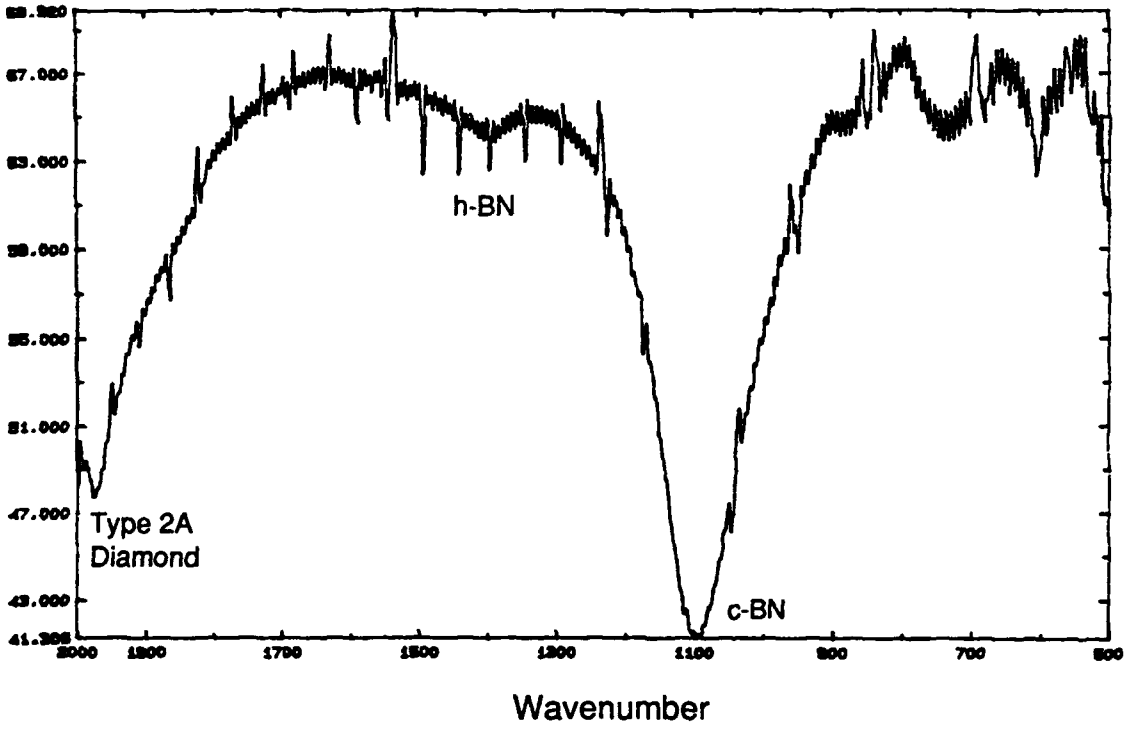

Figure 2. FTIR spectrum of BN film on single crystal diamond.

SEM of the sample deposited at 400°C showed some cracking of the film in spots. The film deposited at 600°C did not show any cracking or delamination. Films deposited at the same deposition conditions and the same thickness on Si are found to have major cracking and delamination of the BN film.

High resolution TEM (HRTEM) was performed on the samples, and the images are shown in Figs. 3 and 4. It can be seen on these two images that the same type of layered structure observed on BN grown on Si is present, if not as pronounced. On the 400° image the hexagonal and cubic regions appear more intermixed.

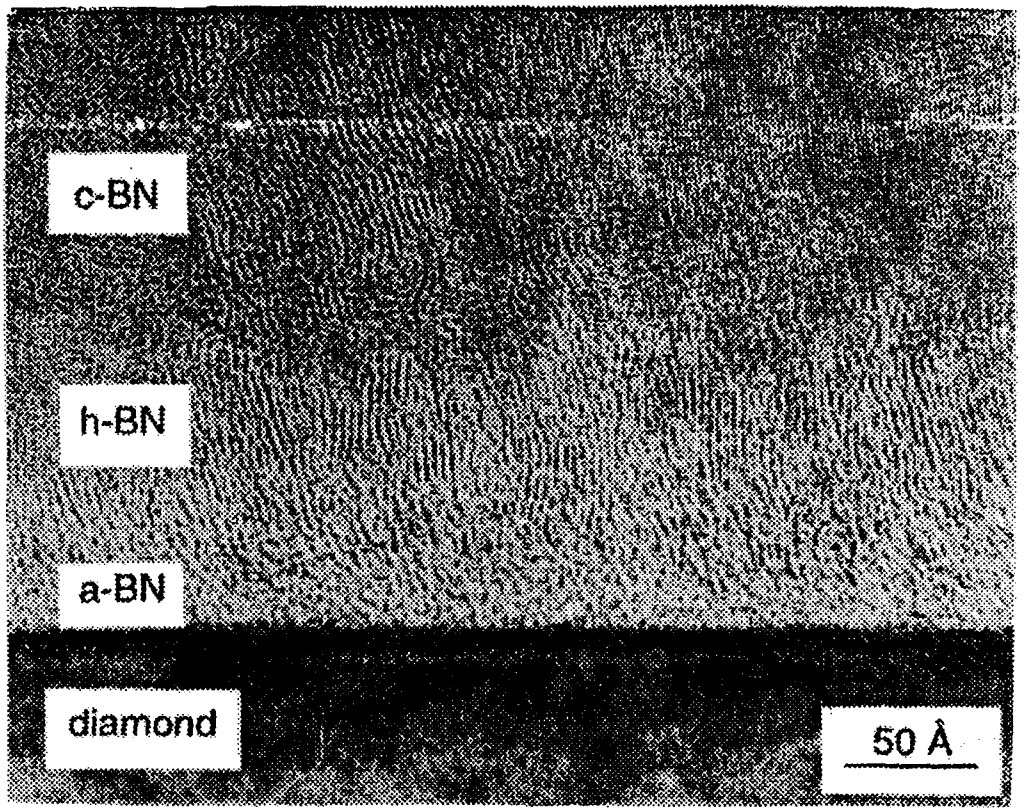

Figure 3. HRTEM of BN on diamond, grown at 400°C

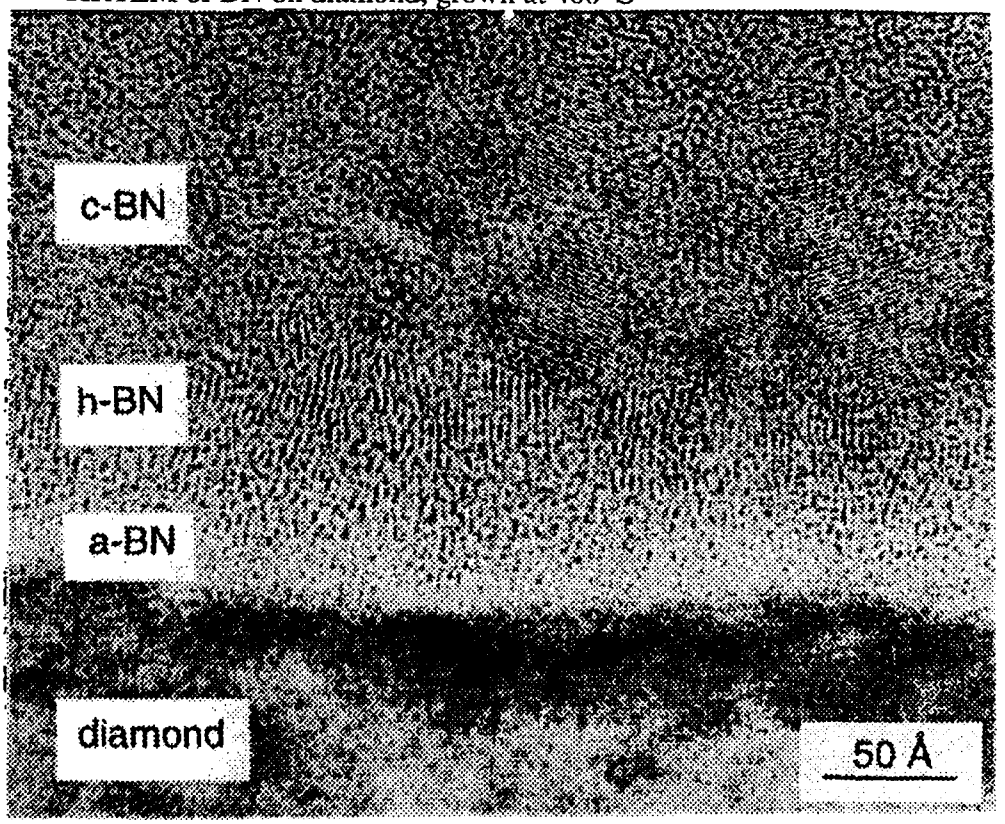

Figure 4. HRTEM of BN on diamond, deposited at 600°C

BN on diamond films

1000 Å of BN was grown on diamond thin films. The diamond films were grown on Si substrates using a microwave CVD process with 1% CH_4 and were 2-4μm thick. Before the c-BN deposition the substrates with the diamond films were etched in a boiling acid solution as described above.

HRTEM was performed on the films, however due to the roughness of the diamond surface a clear image could not be obtained. Therefore diamond films on silicon on which the diamond surface had been polished smooth were acquired and 1000 Å BN deposited on those. SEM of the films showed the presence of what appeared as black spots on the surface of the films. It is not yet clear what the source of the spots is, although they may be due to holes in the BN film brought about by the ion bombardment. HRTEM of these films will occur in the near future.

Raman spectroscopy was also performed on these films. The c-BN peak was not observed. This is not unexpected, as getting the Raman peak generally requires more crystallinity than we have been able to achieve.

Diamond films on BN films

Diamond films were grown on BN films which had been deposited on Si substrates. The thickness of the BN films was 150Å. This was thick enough that the surface of the film would be cubic, but not thick enough for delamination to be a problem. The diamond was grown on these BN films using substrate biasing to help in nucleation of the diamond, as described in Ref. 11. Observation of the plasma during diamond growth showed the plasma to be an unusual color, which may indicate that the BN was being etched during the initial diamond growth, due to bombardment. SEM of the sample showed diamond to have formed on areas of the substrate. It is not clear whether the diamond growth occurred on the BN or on areas where BN had been etched off.

We are presently growing new diamond films on BN films without using the substrate biasing. This is being done on three different thicknesses of BN film: 20Å, 50 Å, and 150Å. These thicknesses correspond to the thicknesses at which the BN surface is amorphous, hexagonal, and cubic, respectively. These experiments may give information on how diamond nucleates on the different BN phases.

BN on Si

XPS. BN films were grown on Si and XPS was performed on them. Films were 20 Å and 100 Å thick. Other than thickness, deposition conditions were identical. The XPS could get data on the top 50 Å of the film, this allowed us to compare the Si-BN interface with the BN material in the film at 50-100Å. It is seen in Fig. 5 that at the interface there are both Si-Si

(99 eV) and Si-N bonds (101 eV) present. This indicates that there is not an abrupt transition from the Si substrate to the BN film, but that the nitrogen ion bombardment causes the formation of an interfacial silicon nitride (Si_3N_4) layer.

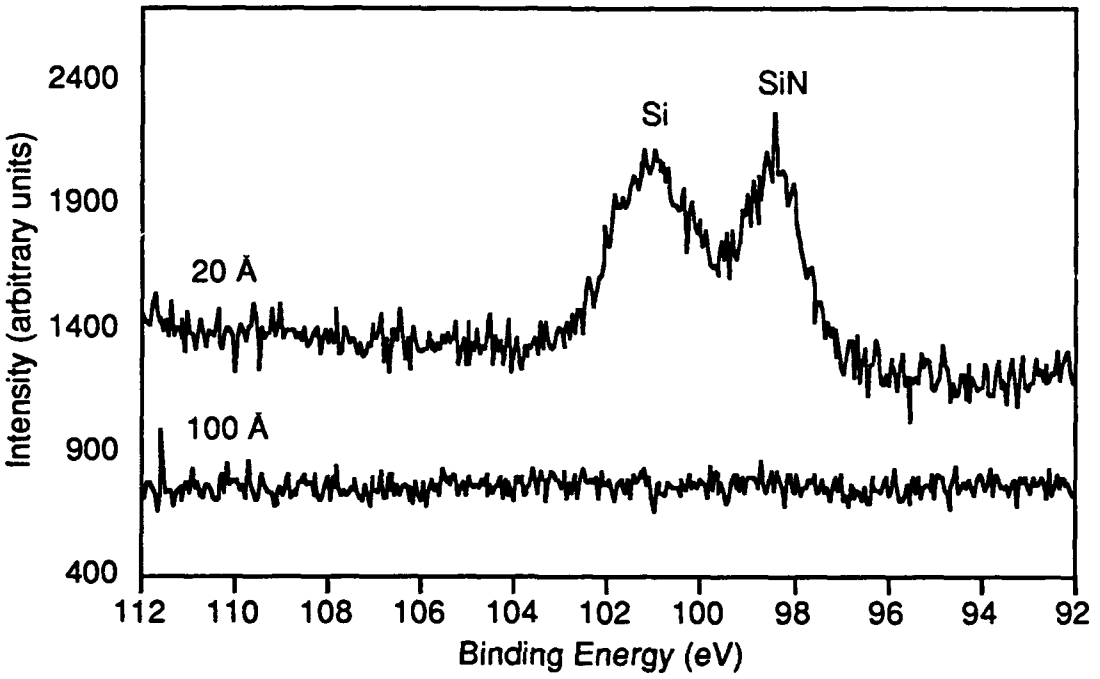

Figure 5. XPS spectra showing Si peaks on 20Å and 100Å thick films.

In Figure 6 the boron XPS peaks for the two films are shown. It is seen that on the 100 Å film the peak due to BN is present. On the 20 Å film there is the BN peak, but also a shoulder that appears to be due to the elemental B peak. This would indicate that near the interface there is both N bonded and B bonded B present.

Figure 7 shows the XPS peaks for Ar. It is seen that there is not much difference between the film at 20 Å and at 100Å. Both contain a detectable amount of Ar.

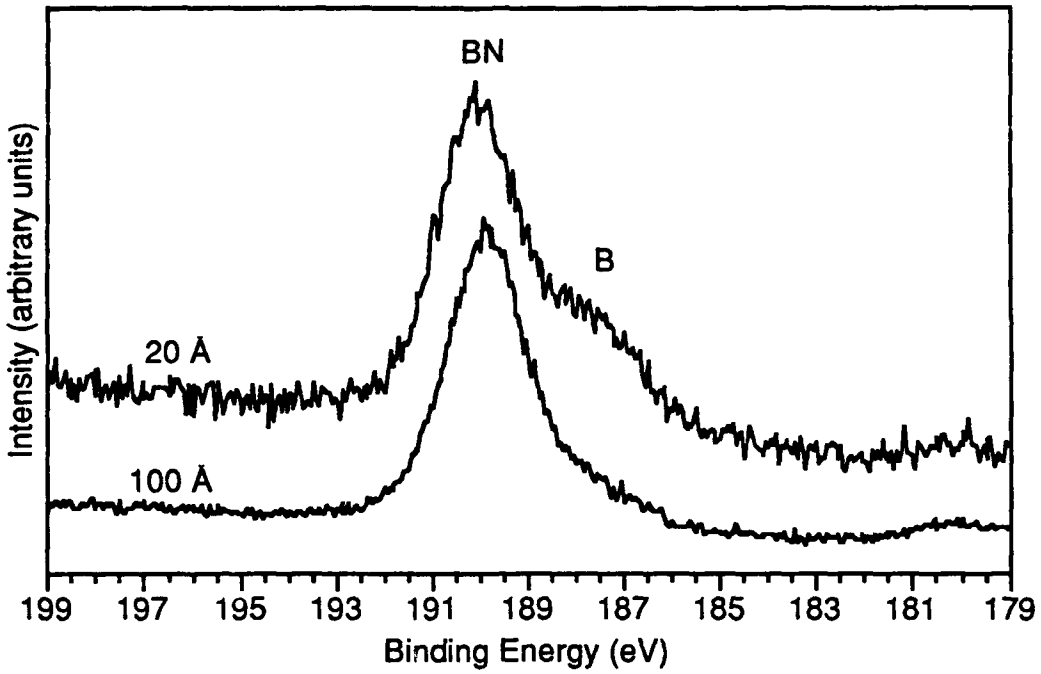

Figure 6. XPS spectra showing B peaks on 20Å and 100Å thick films.

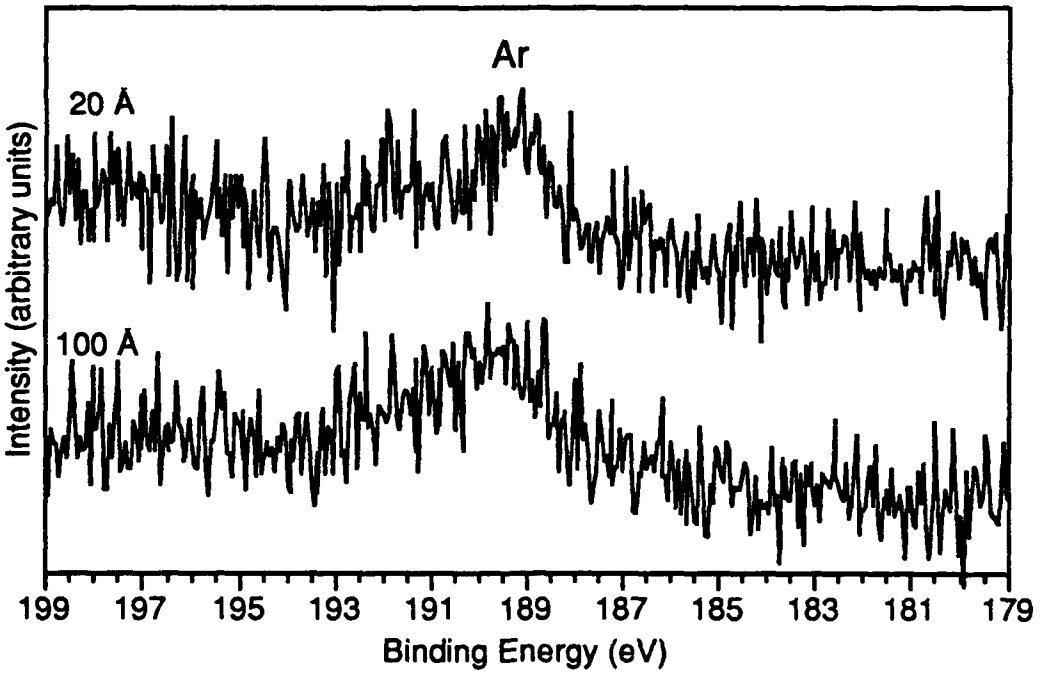

Figure 7. XPS spectra showing Ar peak on 20Å and 100Å thick films.

RBS. For RBS it is preferred that the substrate material have a lower atomic number than the film material. Otherwise the spectrum of the substrate will overlap that of the film material, making the film spectra difficult to read. Therefore the film for RBS was deposited on a Be

substrate. Results are shown in Figure 8. RBS is more sensitive to materials of higher atomic numbers, due to their larger nuclear cross sections. Therefore, the size of the peaks of the materials at various channel numbers does not directly show their actual concentration. Computer modeling of the spectra showed that in addition to the expected Be, B, and N, there is also O at the Be surface, and Ar, Fe, and Hf present in the film. The modeling indicates that the O peak is due to a BeO layer between the Be substrate and BN film, and that the atomic percentage of Ar was ~1.5%, of Fe ~0.2%, and of Hf ~0.05%. The source of the Ar would be the Ar ion bombardment during growth, the Fe is probably due to the ion beam bombarding the stainless steel shutter above the substrates, sputtering Fe onto the film. The Hf may be due to the deposition system also being used for Hf film deposition, and previously deposited Hf from the substrate block being sputtered.

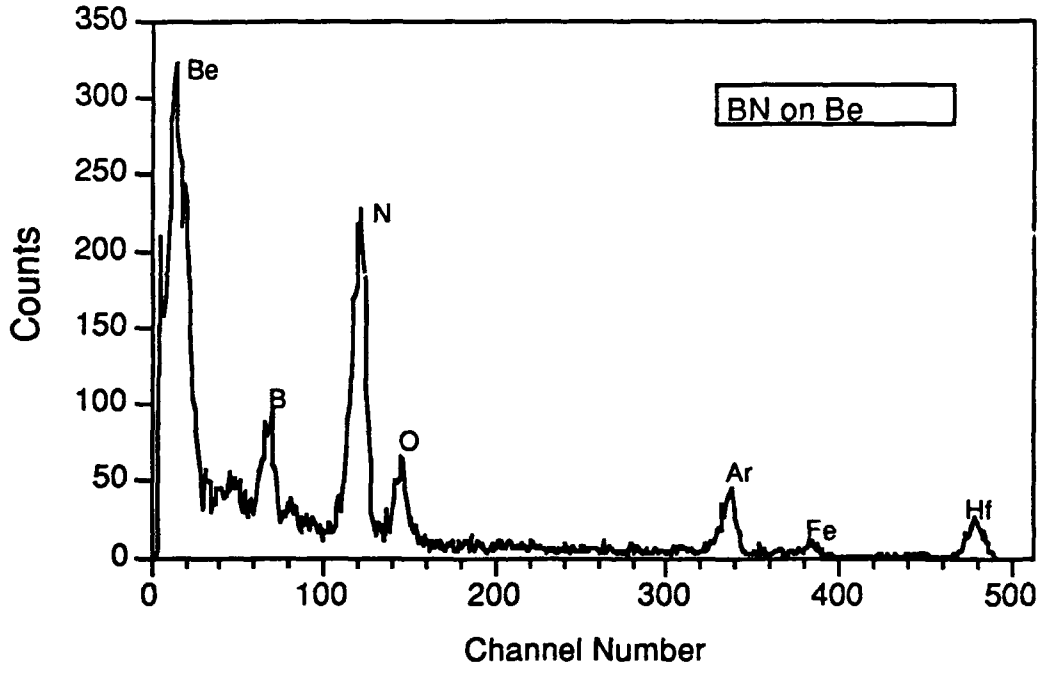

Figure 8. RBS spectra of BN film on Be substrate.

Growth of initial boron layer. The XPS analysis showed that an initial Si_3N_4 layer was forming at the Si surface. It was thought that the formation of this layer may be inhibiting the epitaxial growth of c-BN. Therefore attempts were made to deposit an initial boron layer before starting the ion bombardment. Boron layers of 20 Å, 50 Å, and 100 Å were deposited under conditions found to lead to cubic growth. FTIR examination of the films showed that all still had a significant h-BN component.

Other substrates. Ni and Cu have lattice spacing very close to that of c-BN. Therefore it was thought that they may be better substrates for c-BN than Si which has a lattice mismatch of 34%. Reflectance FTIR was performed on these films.

Films were grown under conditions which had been found to give c-BN films on Si. Films grown on the Ni substrate were found to be mixed h-BN and c-BN (Figure 9); films grown on Cu were h-BN with no evidence of the presence of c-BN (Fig. 10).

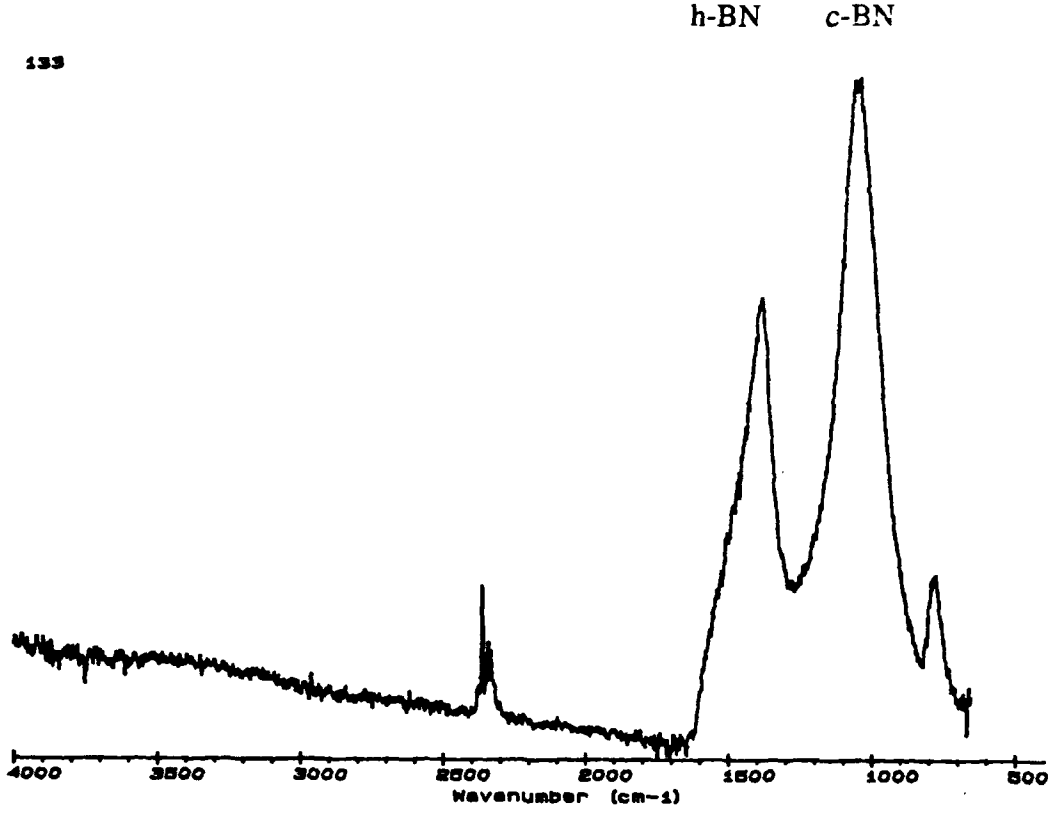

Figure 9. Reflectance FTIR of BN film on Ni substrate.

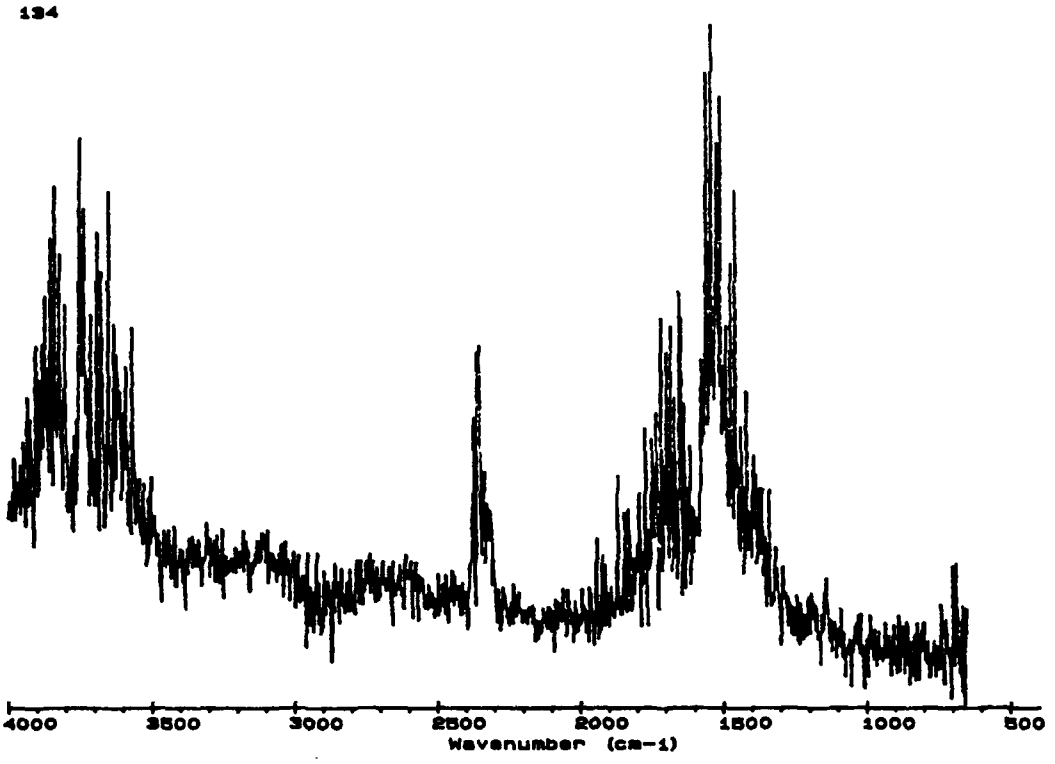

Figure 10. Reflectance FTIR of BN film on Cu substrate.

Patterned substrates

Selected area deposition was performed on patterned Si substrates. These consisted of Si wafers which had been coated with an SiO_2 layer. Holes were etched into the SiO_2, to expose the Si in regions of varying diameters. Examination by SEM showed that good adhesion of the BN film on the Si occurred within the etched holes. The material deposited on the SiO_2 around the holes, had poor adhesion.

D. Discussion

The results shown in the paper in Appendix A demonstrate that cubic boron nitride grows on Si with an initial amorphous layer, followed by a hexagonal layer, followed by the growth of cubic material. The fact that the phase changes at some point in the film growth to the metastable cubic phase indicates that at the non-equilibrium deposition conditions used, cubic is the stable phase. This leads to the question of why the film growth is not cubic, but is initially amorphous, and whether it is at all possible to grow epitaxial c-BN. The lack of any repeatable examples of epitaxial c-BN in the literature raises the same question. It was initially thought that the problem was due to the poor lattice mismatch between Si and c-BN. However the results obtained using other substrates with excellent lattice matching showed this not to be the case. It has previously been predicted that c-BN can grow epitaxially on diamond [12]. Yet a

layered structure similar to that observed on Si was also seen on films grown on diamond substrates. Depositions on Cu (with an exact lattice match to c-BN) and on Ni also gave mixed phase films. The fact that depositing an initial layer of boron did not improve the films also indicates that the Si/BN interface itself may not be the problem.

The results presented in Appendix A showed that there is not a sharp change at the interface from Si to cubic BN. The XPS results that there is both Si_3N_4 and elemental B (B bonded to other B, not to N) at the interface show that not only is there not a sharp transition to cubic phase BN, but that there is not a sharp transition from Si to BN of any phase. For epitaxial c-BN a sharp Si to BN transition would be the first requirement. The ion bombardment itself, while apparently necessary to grow c-BN [13] may in itself be preventing the growth of epitaxial c-BN by forming a Si_3N_4 layer.

Recent work [14] suggests that c-BN forms due to the buildup of stress in the growing films. That study suggests that the onset of the cubic phase will not be initiated until the compressive stress is high enough, which will not occur until a certain film thickness is reached. Our results appear to confirm this.

The actual mechanism causing the stress in the film is not clear. It may be densification due to the ion bombardment. Densification and associated stress has been previously observed in ion bombarded films [15]. The densification occurs through the collapse of the void structure found in non-bombarded films. The stress may also be due to the presence of interstitials in the film. In the case of the c-BN films, the relatively high concentration of Ar (1.5 at.%) as shown by RBS and XPS suggests that the compressive stress may be caused by interstitial Ar atoms.

E. Conclusions

HRTEM and FTIR studies have revealed that BN growth on Si(100) substrates occurs as a single sequence of thin amorphous, hexagonal and cubic layers. The c-BN is single phase and does not undergo further transformation to a thickness of ≈1000Å.

c-BN did not grow epitaxially on any substrate. This may be due to the need for a certain level of compressive stress in the films before the initiation of the cubic phase. This compressive stress would not be reached until the film has grown to a certain thickness (50-100Å). The cause of the compressive stress may be interstitial Ar in the film.

F. Future Research Plans/Goals

Work is continuing on depositing BN on diamond films. We are obtaining a number of oriented 100 diamond films, to use as substrates. This will allow the growth of films at a wider range of deposition conditions then we were able to do on single crystal diamonds. The effect of both substrate temperature and bombardment level will be examined.

BN films on Si have been deposited at different thicknesses which will give different BN phases at the film surface. Diamond films are being grown on these and the effect of the different BN phases on diamond nucleation is being studied.

We are in the process of doing a systematic study of the effect of substrate temperature on the growth of BN on Si. Films are being characterized by FTIR and HRTEM.

Auger electron spectroscopy will be used to examine the first 200 Å of a BN film, to see how the composition varies with thickness. This may give some insight into how the phase evolution of the film develops.

The effect of post-deposition annealing will be studied. It will be seen if this has any effect on the structure of the films.

G. References

1. J. Thomas, Jr., N. E. Weston, and T. E. O'Conner, J. Am. Chem. Soc. **84**, 4619 (1963).
2. R. H. Wentorf, Jr., J. Chem. Phys. **26**, 956 (1957).
3. F. Shimokawa, H. Kuwano, and K. Nagai, Proc. 9th Symp. on ISIAT 85 Tokyo (1985).
4. K. Inagawa, K. Watanabe, H. Ohsone, K. Saitoh, and A. Itoh, J. Vac. Sci. Technol. **A5**, 2696 (1987).
5. Y. Andoh, K. Ogata, and E. Kamijo, Nucl. Instrum. Methods Phys. Res. **B33**, 678 (1988).
6. M. Murakawa and S. Watanabe, Surf. Coat. Technol. **43/44**, 128 (1990).
7. H. Saitoh, T. Hirose, H. Matsui, Y. Hirotsu, and Y. Ichinose, Surf. Coat. Technol. **39/40**, 265 (1989).
8. R. Geick and C. H. Perry, Phys. Rev. **146**, 543 (1966).
9. P. J. Gielisse, S. S. Mitra, J. N. Plendl, R. D. Griffis, L. C. Mansur, R. Marshall, and E. A. Pascoe, Phys. Rev. **155**, 1039 (1967).
10. C. H. Carter, Jr., J. A. Edmond, J. W. Palmour, J. Ryu, H. J. Kim and R. F. Davis in *Microscopic Identification of Electronic Defects in Semiconductors*, edited by N. M. Johnson, S. G. Bishop, and G. Watkins (Mater. Res. Soc. Proc., **46**, Pittsburgh, PA 1985) pp. 593 -598.
11. B. R. Stoner, G.-H. M. Ma, S. D. Wolter, and J. T. Glass, Phys. Rev. B, **45**, 11067 (1992).
12. M. W. H. Braun, H. S. Kong, J. T. Glass, and R. F. Davis, J. Appl. Phys. **69**, 2679 (1991).
13. D. J. Kester and R. Messier, J. Appl. Phys., **72**, 504 (1992)
14. D. R. McKenzie, talk given at the 1992 American Vacuum Society annual meeting, Chicago, IL, November 1992.
15. R. A. Roy and D. S. Yee, in *Handbook of Ion Beam Processing Technology*, edited by J. J. Cuomo, S. M. Rossnagel, and H. R. Kaufman, (Noyes, Park Ridge, NJ, 1989).

VI. Phase Evolution in Boron Nitride Thin Films*

D. J. Kester, K. S. Ailey, K. L. More, and R. F. Davis

Department of Materials Science and Engineering, North Carolina State University, Raleigh, NC 27695

Boron nitride (BN) thin films were deposited on monocrystalline Si (100) wafers using electron beam evaporation of boron with simultaneous bombardment by nitrogen and argon ions. The effect of film thickness on the phase of BN was investigated using Fourier transform infrared (FTIR) spectroscopy and high resolution transmission electron microscopy (HRTEM). These techniques revealed the consecutive deposition of an initial 20Å thick layer of amorphous BN, 20-50Å of hexagonal BN having a layered structure, and a final layer of the cubic phase. The growth of the non-cubic layers are believed to act as a residual stress relief mechanism and/or to form surface and interface relationships which become favorable for the nucleation of the cubic phase. The presence of the amorphous and hexagonal regions may also explain why there have been no reports of the growth of 100% cubic boron nitride on Si.

*Submitted for publication to the Journal of Materials Research

Boron nitride is similar to carbon in having three crystalline structures:[1] a layered hexagonal structure (*h*-BN) corresponding to graphite, the cubic structure (*c*-BN) analogous to diamond, and a rare hexagonal wurtzite structure (*w*-BN) corresponding to Lonsdaleite. The last two phases are metastable under normal environmental conditions. An amorphous phase (*a*-BN) is also common in films and coatings.

The extreme mechanical and thermal properties of *c*-BN make it useful for wear-resistant tools for the machining of steels, for corrosion resistant and electrically insulating parts, and for heat sinks for electronic devices. It has also recently been shown that bulk single crystals of this wide bandgap ($E_g \approx 6.4$ eV) semiconductor can be doped with both n- and p-type impurities and that light emitting p-n junctions can be produced [2]. This phase combined with other BN phases, has also been achieved in thin film form via physical vapor deposition [3-5] and chemical vapor deposition [6] methods.

Most researchers growing BN films use FTIR spectroscopy for phase identification. The cubic phase of BN has a distinct absorption peak at about 1080 cm^{-1}. The hexagonal, turbostratic (disordered hexagonal), and amorphous phases have primary and secondary absorption peaks at 1370 and 780 cm^{-1}, respectively. Thus, these non-cubic phases cannot be distinguished using FTIR. A commonly reported feature of these spectra obtained from analyses of the total thickness of the films wherein the presence of *c*-BN is apparent is the indication of various amounts of the hexagonal and/or amorphous phases (see, e.g., Refs. 4, 5). The FTIR spectra of the films obtained in the present research showed similar results. However, the unusual evolution of these phases has been determined by HRTEM and has been correlated with the FTIR results.

The Si (100) substrates used in the present study received a standard RCA cleaning [7] which included a 5 min. dip in 10% HF as the final step. This left the surface H-terminated and reduced the rate of reaction of this surface with H_2O and O_2 in the atmosphere. The substrates were subsequently transferred to the deposition chamber and heated to 400°C under UHV conditions. Base and deposition pressures were typically $<10^{-9}$ Torr and 10^{-4} Torr, respectively. The growth method involved the electron beam evaporation of B sufficient to achieve a deposition rate of 0.25 Å/s, as measured via a quartz crystal rate monitor. The growing films were simultaneously bombarded with a 0.12 mA/cm^2 ion flux (measured using a biased probe) of 500 eV nitrogen and argon ions produced in a Kaufman source using a 50:50 gas flow ratio of Ar/N_2. A shutter was used to cover the substrate prior to film deposition while the boron evaporation and ion bombardment were brought to correct levels for deposition and allowed to stabilize. Conditions during each deposition were maintained constant. The total film thickness ranged from 125-500Å.

FTIR was performed using an Analect Instruments model fx-6260 spectrometer. Transmission spectra were taken through the BN films and Si substrates. A spectra of an

uncoated Si wafer was taken as a background scan, and the spectra of the coated wafer was ratioed against it. The spectra for films deposited under identical conditions except for growth time are shown in Fig. 1. Peak heights were maximized on each of the spectra, thus only the ratio of peak heights within a single spectra are meaningful; absolute peak heights on different spectra cannot be compared. The relative amount(s) of non-cubic phase(s) was high for very thin films (<200Å). As the deposition time and resulting thickness increased, the relative percentage of the cubic phase increased. This indicated that the ratio of the concentration of the *c*-BN phase to that of the *a*-BN and *h*-BN phases increased as a function of film thickness rather than being constant regardless of deposition time.

To test this hypothesis, structural characterization of the films as a function of thickness was performed via HRTEM using a TOPCON EM-002B microscope operated at 200kV. Cross-sectional samples of the BN films were prepared using standard techniques [8]. The HRTEM images, an example of which is shown in Fig. 2, supported the above hypothesis in that they revealed that three distinct regions had deposited in the following sequence: an initial layer of about 20Å of *a*-BN at the Si (100) interface, a layer of 20-50 Å of *h*-BN, and a top layer of polycrystalline, random oriented cubic material. The hexagonal layers grew perpendicular to the Si (100) surface. An optical diffraction pattern was obtained by performing a Fast Fourier Transform on the HRTEM image to obtain the diffraction information shown in Fig. 3. The lattice spacings for the top layer matched that of *c*-BN, while those within the middle layer matched that of *h*-BN.

As noted above, all reported transmission FTIR spectra obtained from analyses of the total thickness of BN films have indicated the presence of some non-cubic phase. Explanations for this phenomenon include: (1) the occurrence of the non-cubic phases(s) on the grain boundaries within the *c*-BN matrix; (2) separate *h*-BN or *a*-BN micro-regions distributed throughout the films; and (3) a layered sequence of these various phases. Microstructures produced by combinations of these three factors may also exist in the films. The results of the present research indicate that sequential layers of *a*-BN and *h*-BN are the sources of the non-cubic phases. The HRTEM image shows that once the growth of the cubic phase is initiated, this layer is single phase. More specifically, even non-cubic grain boundary regions were not observed. Upon nucleation, the cubic phase grows without further transformation, at least to the maximum layer thickness thus far deposited (≈1000Å).

The exact reason(s) for the occurrence and layer sequence within the microstructure shown in Fig. 2 is (are) not known. Previous work on BN film growth [9] has shown that, for a given substrate temperature, the deposition of a particular phase is a function of momentum transferred into the film by the ion bombardment. The deposition conditions used in this study were those that previously resulted in the growth of films containing substantial concentrations of *c*-BN. However, nucleation of this phase is obviously not automatic. The amorphous

phase may occur initially as a transition zone of reduced residual stress relative to that which would develop during *epitaxial* growth of *c*-BN (or *h*-BN) on Si(100) due to the large mismatch in lattice parameter (≈33.4 % for *c*-BN). This constraint may be joined or surmounted by the constraint of surface energy. It may be impossible for *c*-BN (or even h-BN) to nucleate and grow *epitaxially* on Si(100) due to the much larger surface energy of the BN crystalline phases.

The transformation of the *a*-BN to the *h*-BN phase is not surprising from the viewpoint of equilibrium thermodynamics under standard conditions. However, as noted above, the experimental parameters favored the nucleation of *c*-BN. The explanation for the nucleation of *h*-BN may be found in the atomic structure of the *a*-BN. X-ray radial distribution curves normally show that stoichiometric amorphous phases are similar in atomic arrangement to their crystalline analogs, especially among nearest neighbors and occasionally to even greater spheres of coordination. The essentially indistinguishable IR spectra between *a*-BN and *h*-BN also indicate similar atomic arrangements in these two phases which may explain the subsequent nucleation of this phase. The reason for the preferred orientation of the basal plane of the *h*-BN perpendicular to the Si(100) surface is not known, though it may also be related to the atomic structure of the *a*-BN surface.

A three dimensional phase transformation only at the growing surface of a thin film phase normally considered to be the equilibrium structure (*h*-BN) to one which is metastable (*c*-BN) is truly an anomaly even under highly nonequilibrium conditions. The experimental conditions coupled with the presence of the high surface energy edges of the *h*-BN which acted as the substrates are believed to be the reasons for this unusual transformation. If this is the case, it would be analogous to the recent findings regarding nucleation of diamond on non-diamond substrates. Williams [10] has investigated personally and via review of the literature the sequence of deposition events leading to the onset of diamond nucleation on carbide- and noncarbide-forming substrates. In all documented cases, the deposition of a particulate amorphous and/or graphitic phase preceded the nucleation of diamond. Davis has argued [11] that the high energy edges of appropriately oriented graphite or other C particles are the likely sites for the onset of diamond nucleation (this scenario may also explain the considerable effectiveness of scratched substrates in that the scratches act to orient the C particles such that diamond nucleation is favored). The research of Angus and his colleagues [12, 13] concerned with the nucleation and growth of diamond on various orientations of pyrolytic graphite support this hypothesis. In this regard, recent research by the present authors involving the deposition and HRTEM of BN films on (100) single crystal diamond substrates under the same conditions noted above resulted in the initial deposition of a very thin *a*-BN layer and a subsequent layer containing a mixture of primarily *c*-BN and a small amount of *h*-BN. The details of this study will be reported in the near future.

Finally, a close examination of Fig. 2 reveals an uneven *h*-BN/*c*-BN interface but a very smooth *c*-BN surface. This indicates that (1) the initial nucleation of the c-BN did not occur simultaneously across the *h*-BN surface and (2) the deposition rate of these two phases is essentially the same. These results also show that *c*-BN does not form due to the elimination of the *h*-BN phase by the ion beam. The HRTEM results clearly show that the *h*-BN phase forms under the same conditions used to deposit *c*-BN. To date, it has not been possible to determine the orientation relationship between the *h*-BN and the *c*-BN phases at the site of nucleation.

In summary, HRTEM and FTIR studies have revealed that BN growth on Si(100) substrates occurs as a single sequence of thin amorphous, hexagonal and cubic layers. The *c*-BN is single phase and does not undergo further transformation to a thickness of ≈1000Å. The non-cubic layers are believed to occur initially to form relatively relaxed transition zones and/or to achieve a surface and interface energy relationship which eventually becomes favorable to the nucleation of the *c*-BN. The preferred orientation of the *h*-BN layers and the exposure of the high surface energy edges of this phase are believed to act in tandem with the highly non-equilibrium growth conditions to achieve the deposition of the *c*-BN.

Acknowledgments

The authors express their appreciation to the Electronic Materials Center of Kobe Steel, USA and the Strategic Defense Initiative through the Office of Naval Research and via the contract #N00014–92–J-1720 for support of this research and to Professor J. Angus of Case Western Reserve University for the information regarding the deposition of diamond on pyrolytic graphite and for giving us a preprint of the paper describing this research. A portion of the electron microscopy was supported as part of the Ceramic Technology for Advanced Heat Engines Program of the Advanced Materials Development Program and partially performed in the HTML User Facility, both sponsored by the U. S. Department of Energy, Assistant Secretary for Conservation and Renewable Energy, Office of Transportation Technologies, under contract DE AC0584OR021400 managed by Martin Marietta Energy Systems, Inc.

References

[1] L. Vel, G. Demazeau and J. Etourneau, Mater. Sci. and Eng. **B10**, 149 (1991).

[2] O. Mishima, K. Era, J. Tanaka, and S. Yamaoka, Appl. Phys. Lett., **53**, 962 (1988).

[3] K. Inagawa, K. Watanabe, H. Ohsone, K. Saitoh, and A. Itoh, J. Vac. Sci. Technol. **A5**, 2696 (1987).

[4] Y. Osaka, M. Okamoto, and Y. Utsumi, Mater. Res. Soc. Symp. Proc., **223**, 81 (1991).

[5] N. Tanabe, T. Hayashi, and M. Iwaki, Diamond Relat. Mater., 1, 151 (1992).

[6] H. Saitoh, T. Hirose, H. Matsui, Y. Hirotsu, and Y. Ichinose, Surf. Coat. Technol. **39/40**, 265 (1989).

[7] W. Kern and D. A. Puo-tinen, RCA Rev. **31**, 187 (1970).

[8] C. H. Carter, Jr., J. A. Edmond, J. W. Palmour, J. Ryu, H. J. Kim and R. F. Davis in *Microscopic Identification of Electronic Defects in Semiconductors*, edited by N. M. Johnson, S. G. Bishop, and G. Watkins (Mater. Res. Soc. Proc., **46**, Pittsburgh, PA 1985) pp. 593 -598.

[9] D. J. Kester and R. Messier, J. Appl. Phys., **72**, 504 (1992)

[10] B. E. Williams, Ph. D. Dissertation, North Carolina State University, 1992

[11] R. F. Davis, Presentation at the 1991 Gordon Conference on Inorganic Thin Films.

[12] J. Angus (private communication).

[13] Z. Li, L. Wang, T. Suzuki, P. Pirouz and J. C. Angus, in press.

FIGURES

1. FTIR spectra of BN films of various thicknesses all deposited on Si (100) substrates under the following conditions: Boron deposition rate: 0.25 Å/s; ion energy: 500 eV; ion flux: 0.12 mA/cm^2; ion bombardment by 50:50 Ar:N_2; substrate temperature: 400°C.
2. Cross-sectional HRTEM image of BN film showing Si substrate and regions of amorphous BN (a-BN), hexagonal BN (h-BN), and cubic BN (c-BN).
3. Optical diffraction pattern from the HRTEM image of Fig. 2. (a) From the region labeled as h-BN. (b) From the region labeled as c-BN.

Figure 1

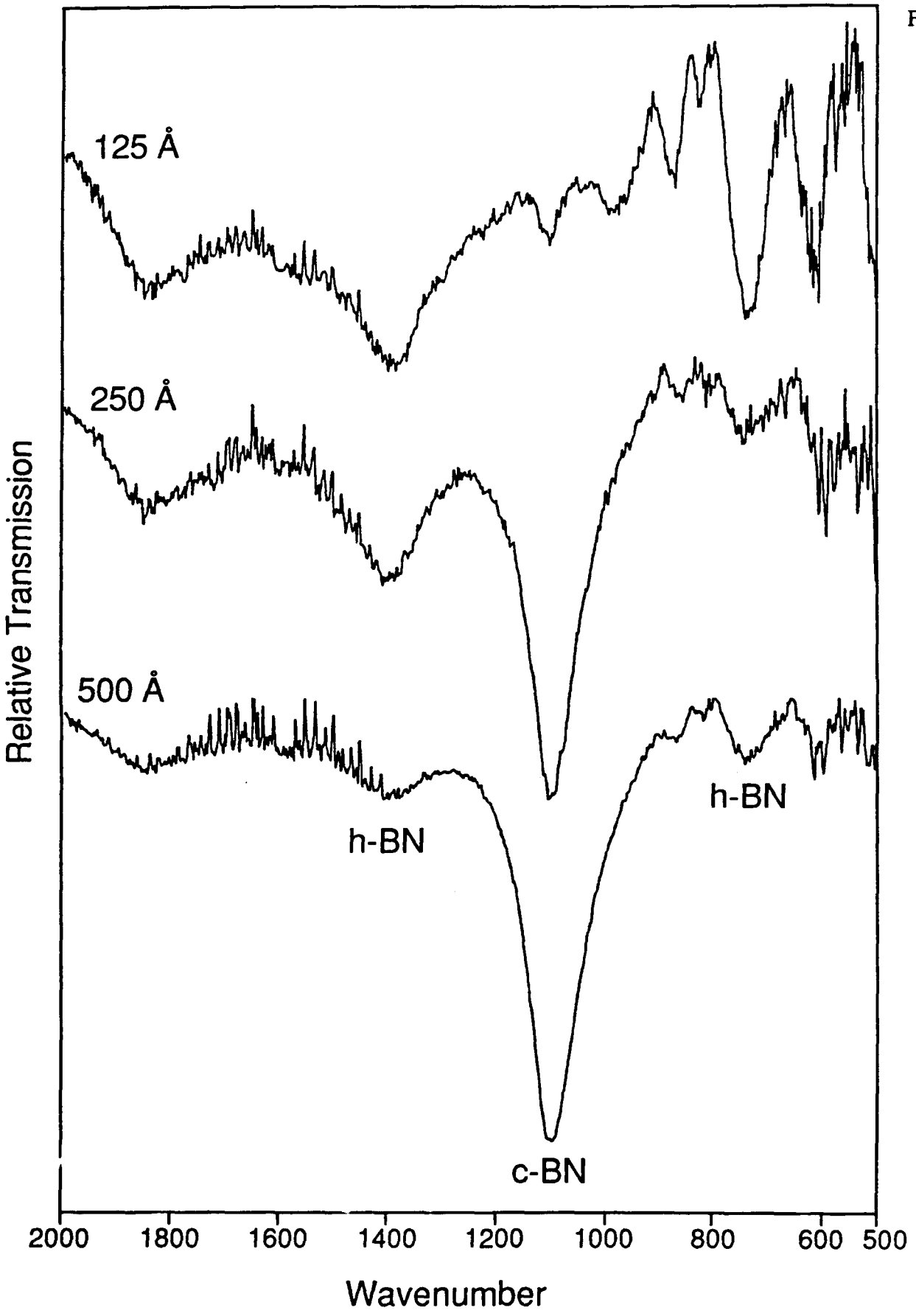
125 Å
250 Å
500 Å
h-BN
h-BN
c-BN
Relative Transmission
2000
1800
1600
1400
1200
1000
800
600
500
Wavenumber

Figure 2

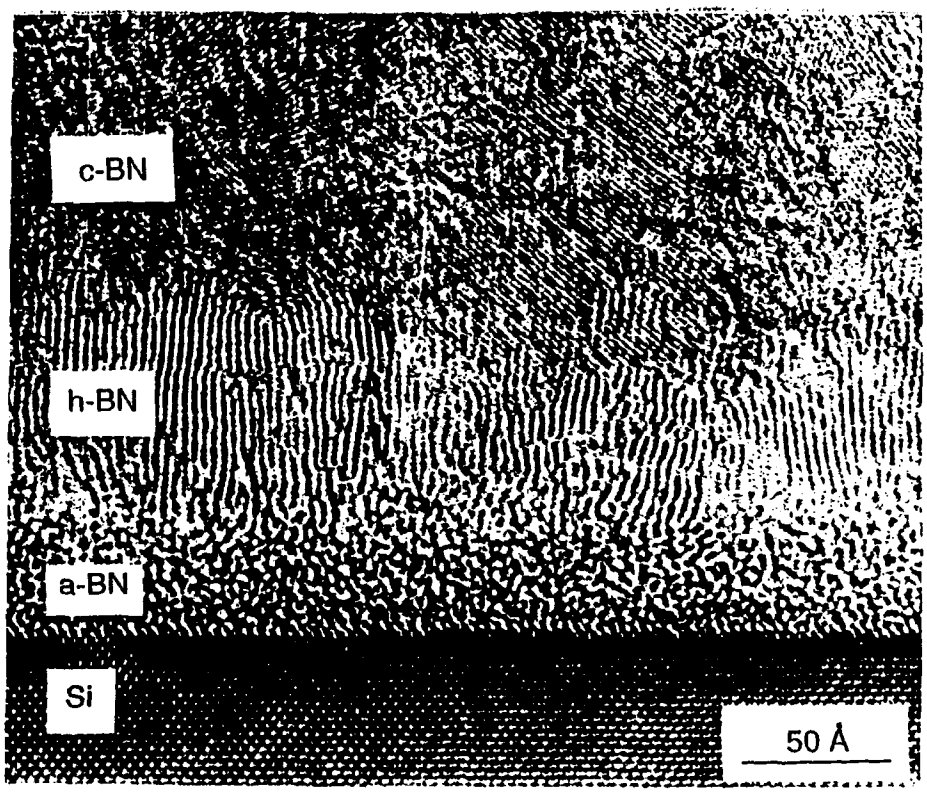

Figure 3

(a)

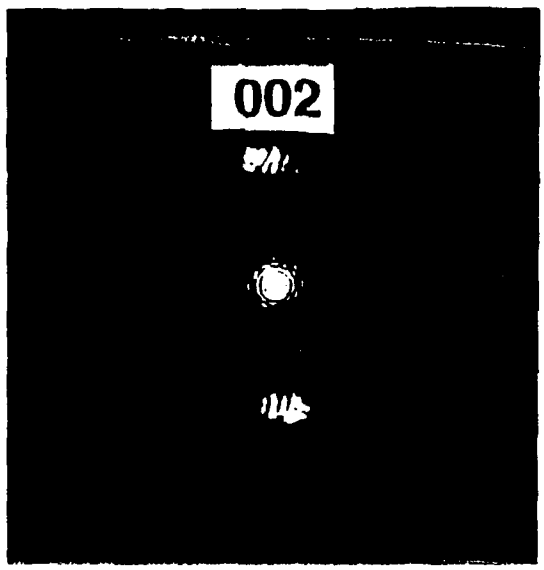

(b)

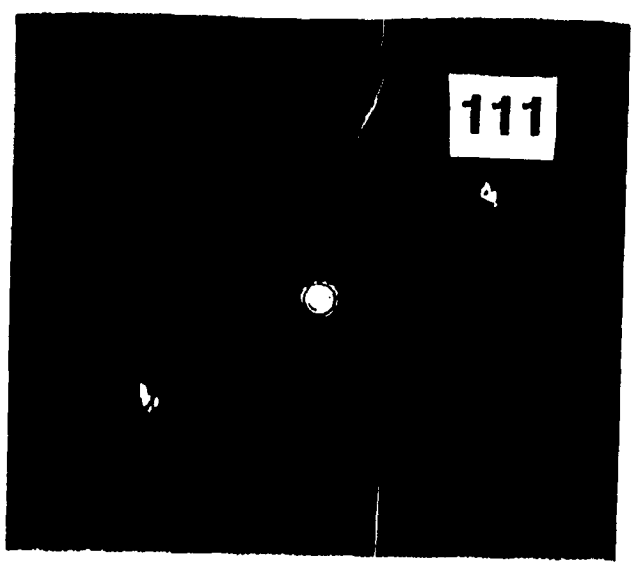

VII. Distribution List

Mr. Max Yoder Office of Naval Research Electronics Division, Code: 1114SS 800 N. Quincy Street Arlington, VA 22217-5000	3
Administrative Contracting Officer Office Of Naval Research Resident Representative The Ohio State University Research Center 1960 Kenny Road Columbus, OH 43210-1063	1
Director, Naval Research Laboratory ATTN: Code 2627 Washington, DC 20375	1
Defense Technical Information Center Bldg. 5, Cameron Station Alexandria, VA 22314	12